Combining Digital Imaging and Genome Wide Association Mapping to Dissect Uncharacterized Traits in Plant/Pathogen Interactions

Rachel F. Fordyce[1], Nicole E. Soltis[1], Celine Caseys[1], Raoni Gwinner [1], Jason A. Corwin[1,2], Susana Atwell[1], Daniel Copeland[1], Julie Feusier[1], Anushriya Subedy[1], Robert Eshbaugh[1], and Daniel J. Kliebenstein[1,3*]

[1]Department of Plant Sciences, University of California, Davis, One Shields Avenue, Davis, CA, 95616, USA

[2]Department of Ecology and Evolutionary Biology, University of Colorado, Boulder, 1900 Pleasant Street, Boulder, CO, 80309-0334, USA

[3]DynaMo Center of Excellence, University of Copenhagen, Thorvaldsensvej 40, DK-1871, Frederiksberg C, Denmark

***Correspondence:** Daniel J. Kliebenstein, Department of Plant Sciences, University of California, Davis, One Shields Ave, Davis, CA, 95616, USA.

Kliebenstein@ucdavis.edu

Short Title: Digital Lesion Genetics

Summary: Digital imaging allows the identification of genes controlling novel lesion traits.

Keywords: Plant-pathogen interaction, *Arabidopsis thaliana*, *Botrytis cinerea*, GWAS.

Abstract

Plant resistance to generalist pathogens with broad host ranges, such as *Botrytis cinerea*, is typically quantitative and highly polygenic. Recent studies have begun to elucidate the molecular genetic basis underpinning plant-pathogen interactions using commonly measured traits including lesion size and/or pathogen biomass. Yet with the advent of digital imaging and phenomics, there are a large number of additional resistance traits available to study quantitative resistance. In this study, we used high-throughput digital imaging analysis to investigate previously uncharacterized visual traits of plant-pathogen interactions related disease resistance using the *Arabidopsis thaliana/Botrytis cinerea* pathosystem. Using a large collection of 75 visual traits collected from every lesion, we focused on lesion color, lesion shape, and lesion size, to test how these aspects of the interaction are genetically related. Using genome wide association (GWA) mapping in *A. thaliana*, we show that lesion color and shape are genetically separable traits associated with plant-disease resistance. Using defined mutants in 23 candidate genes from the GWA mapping, we could identify and show that novel loci associated with each different plant-pathogen interaction trait, which expands our understanding of the functional mechanisms driving plant disease resistance.

Introduction

The ability to resist biotic attackers, including plant pathogens, is central to a plant's survival and fitness. This need for resistance is complicated by the immense variety of infection strategies and pathogenic species that can attack an individual plant. These pathogens differ in their lifestyle and host range with each having a different requisite optimal virulence mechanism. Specialist pathogens often co-evolve with host plants to develop virulence strategies targeted on a specific resistance mechanisms within the plant. These biotrophic pathogens must strike a delicate balance between keeping host plant's cells alive by while absorbing nutrients and avoiding detection and suppressing plant defenses. Plant defense against specialists is accordingly tailored to the specific pathogen with which it has been co-evolving, often involving gene products that directly or indirectly recognize effectors or molecular patterns specific to that pathogen. This co-evolutionary link between host and specialist pathogen frequently leads to large-effect, gene-for-gene resistance involving the specific pathogen recognition R-genes (Jones and Dangl, 2006). In contrast, necrotrophic pathogens are often generalists, deploying a diverse array of virulence mechanisms to precisely kill host plant cells (Laluk and Mengiste, 2010). The generalist attack is multifaceted, relying on many different phytotoxins and enzymes working in parallel to subjugate the plant. Host-pathogen co-evolution in generalist pathogens is not well understood because the pathogen can attack innumerable hosts, causing myriad plant species to encounter a similarly dizzying array of generalist pathogen virulence mechanisms. As such, generalist necrotrophic resistance typically has a highly quantitative polygenic basis that involves physical barriers, such cuticle formation and cell wall modification, chemical barriers, such as secondary metabolites or reactive oxygen species, and inducible defenses (Rowe and Kliebenstein, 2008; Laluk and Mengiste, 2010; Windram et al., 2012; Corwin et al., 2016b).

Infected plants display a large variety of interrelated traits during the infection process. The abundance of scientific literature concerning molecular mechanistic analysis of plant-pathogen interactions largely relies either on lesion size (a single number measuring the plant area displaying symptoms) or pathogen biomass within the infected plant tissue. While these

observations are relatively easily measured traits that reflect plant susceptibility to a pathogen, they do not fully describe all aspects of disease resistance within the plant host. For instance, comparing the molecular and quantitative genetic basis of resistance using lesion size versus the underlying biochemical plant resistance responses has shown that different genes can contribute to these traits. This suggests that the lesion size measurements are not providing the full picture of the resistance response (Rowe and Kliebenstein, 2008; Bock et al., 2010; Li et al., 2015; Corwin et al., 2016b; Schwanck and Del Ponte, 2016; Barbedo, 2017; Matsunaga et al., 2017). There has been recent interest in extending our understanding of plant-pathogen resistance by conducting more extensive phenotyping of disease symptoms, including hyperspectral imaging of lesions that records spectra from the visible into the infrared range (Montes et al., 2007; Kuska et al., 2015; Mutka and Bart, 2015; Leucker et al., 2016). This analysis has differentiated between diseases on the same plant through biochemical responses using light spectra from 400nm to 1000nm (Mahlein et al., 2012). These spectra provide a blend of visual symptoms characterized not only by extent of necrosis, but also by water content, pigment modification, tissue function, and appearance of fungal structures (Mahlein et al., 2012). However, the molecular mechanisms controlling these visual and biochemical aspects of the plant-pathogen interaction are largely unstudied, and little is known about their mechanistic basis and how this relates to molecular mechanisms identified using pathogen biomass or lesion size. Therefore, there is a need to study plant-pathogen interactions from the multi-dimensional view that can be provided by digital imaging of lesions and assess how this links to one-dimensional measurement of lesion progression. This could discover new insights into the physiology of pathogen strategy and host response.

One developing model system to directly study the complexity of molecular plant resistance to generalist pathogens can be found within the *Arabidopsis thaliana/Botrytis cinerea* pathosystem (Corwin and Kliebenstein, 2017). *Botrytis cinerea* is a generalist necrotrophic pathogen with a broad range of hosts that includes Bryophytes, through Gymnosperms, to Angiosperms (Jarvis, 1977; Staats et al., 2005; Choquer et al., 2007; Elad et al., 2016). This host range appears to be facilitated by a high level of intraspecific genetic

diversity and elevated levels of recombination in comparison to specialist clonal pathogens (Giraud et al., 1997; Alfonso et al., 2000; Vaczy et al., 2008; Kretschmer et al., 2009; Stefanato et al., 2009; Amselem et al., 2011; Aguileta et al., 2012; Atwell et al., 2015). This natural genetic variation within *B. cinerea* quantitatively affects lesion size within all plants tested, including *A. thaliana* (Rowe and Kliebenstein, 2010; Valiuskaite et al., 2010; Amselem et al., 2011; Corwin et al., 2016a). *A. thaliana* resistance to *B. cinerea* involves key signaling pathways, such as Jasmonate and the BIK/BAK response system (Thomma et al., 1999; Veronese et al., 2006). More recently, high-throughput digital imaging analysis of the *A. thaliana/B. cinerea* interaction has allowed the identification hundreds of genes associated with the size of the lesion, with most genes being associated to one or two isolates (Corwin et al., 2016a). The high-throughput digital imaging pipeline used also can provide additional visual traits that facilitates the comparison of novel visual traits with traditional measures related to disease resistance. We examined a wide array of visual information of lesion traits to find a broad and largely orthogonal subset of visual parameters to measure the interaction, including lesion yellowness, lesion greenness, and lesion shape.

Here, we rely on the natural variation in the host and pathogen for the Arabidopsis/Botrytis pathosystem to measure a variety of novel infection-related traits and to conduct genome wide association (GWA) mapping within the host. Genetic mapping will allow us to identify host genes associated with these novel visual traits and expand our understanding of the genetic architecture of quantitative resistance against generalist pathogens. Previous work has shown that GWA mapping, when applied to the *Arabidopsis thaliana/Botrytis cinerea* pathosystem, can identify genes involved in polygenic susceptibility traits, such as lesion size and camalexin production (Corwin et al. 2016). This approach also does not impart *a priori* assumptions on the genes or mechanisms that may play a role in controlling the trait in question. This is exemplified by the observation that many of the genes identified by GWA mapping in *A. thaliana* have not been previously linked to this pathosystem (Jarvis, 1977; Staats et al., 2005; Choquer et al., 2007; Rowe and Kliebenstein, 2008; Mengiste et al., 2010; Valiuskaite et al., 2010; Amselem et al., 2011; Corwin et al., 2016b; Corwin and

Kliebenstein, 2017). For example, this identified Late-elongating Hypocotyl (*LHY*; *At1g01060*), a key developmental and circadian-regulated gene not previously linked to disease resistance as having a significant effect *on B. cinerea* resistance (Corwin et al., 2016b). In addition to known genes, this approach could identify disease resistance effects in completely novel genes like At4g01860, an uncharacterized Cul4-RING E3 component. This suggests that extending this analysis to other traits may allow the identification of additional new disease resistance loci. Further, this can be directly facilitated by a reanalysis of the digital images collected from the previous study explore other traits related to disease resistance.

Within the current study, we re-analyzed the images collected from our previous work to measure visual aspects of lesion development that are not commonly measured with respect to disease resistance, specifically lesion shape and color. A genome wide association mapping analysis of select traits in Arabidopsis revealed a large compendium of genes associated with lesion size, lesion yellowness, lesion greenness, and lesion shape. GO enrichment analysis showed that there were biological processes specific to subsets of traits rather than processes affecting all of the lesion-associated traits. To validate the results of the GWA mapping, we selected 23 genes associated with one or more of the lesion traits and compared the phenotypes of T-DNA knockout mutants. The validation rate was highest for lesion size, at 60%, and lower for the color and shape traits: 33% for lesion yellowness, 38% for lesion greenness, and 20% for lesion eccentricity. This further demonstrated that the genes affected subsets of lesion traits rather than being specific to all traits. As such, expanding our phenotypic analysis of plant-pathogen interactions to novel visual traits like lesion shape and color can identify different mechanisms than solely focusing on lesion size.

Results

Identification of Alternative Disease Related Traits

Using a custom digital image analysis pipeline, we had previously measured lesion size (area) to identify *A. thaliana* genes controlling lesion size within the *Arabidopsis thaliana/Botrytis cinerea* pathosystem using four diverse pathogen genotypes (Corwin et al., 2016b). This previous study used 96 diverse *A. thaliana* accessions chosen based on similar

flowering time to minimize ontogenic variation, which also decreased population structure and rare alleles within the collection. The host pathogen interaction was digitally recorded within a randomized complete block design over two experiments with 4 independent biological replicates per experiment per genotype. Specific lesion traits were obtained using a digital image analysis pipeline for which we have previously only reported results for lesion size (Corwin et al., 2016b). Using the same images, we adapted our imaging pipeline to quantify 75 different lesion parameters from the infections. These included a wide range of traits from the number of pixels for specific hues within the lesion, lesion perimeter, proportion of leaf the lesion occupied, length of the major and minor axes of the lesion, eccentricity of the perimeter, etc. (Corwin et al., 2016a)(Figure 1). As previously reported, there is a wide range of lesion sizes across the host/pathogen interactions (Figure 1A versus C). In addition to lesion size, there is variation in color both within the lesion and the residual leaf. For example, some host/pathogen interactions have large chlorotic sectors surrounding the lesions (Figure 1A, C and F), while others have less chlorosis surrounding the developing lesion (Figure 1B and E). In previous work, we have shown that the pathogen is limited solely to the developing lesion and these chlorotic regions are systemic plant responses to the infection (Rowe and Kliebenstein, 2008; Corwin et al., 2016a). Even within the lesion there are color variants with some being yellower (Figure 1A) while others have a greener hue (Figure 1D). In addition to lesion color, there is variation in lesion shape with some lesions being highly symmetrical and circular (Figure 1D and F) while others are elongated along the major axis of the leaf, possibly due to extended pathogen growth along the mid-vein (Figure 1A and B). This preferential mid-vein growth has also been previously seen as genetically variable across *B. cinerea* infecting *A. thaliana* (Corwin et al., 2016a). We proceeded to study if these additional measurements of the interaction between the plant and the pathogen were providing unique genetic insight into the virulence outcome that was not readily obtained from solely lesion size.

Hierarchical Clustering Analysis for Trait Selection

To select a subset of traits to study further, we conducted a hierarchical clustering analysis (HCA) and constructed a heat map of the 75 lesion traits across the 96 *A. thaliana* accessions

infected with the different *B. cinerea* isolates (Figure 2). This analysis allowed us to assess the inter-relatedness of these alternate infection traits both with each other, and with lesion size, to determine whether the traits are providing distinct information with respect to each other. The HCA showed extensive variation in all the traits dependent on *A. thaliana* accessions and *B. cinerea* isolates, leading to four major trait clusters (Figure S1). In these clusters, color and shape traits distinctly clustered apart from lesion size, and varied across plant accession. From this plot, we chose to proceed with three distinct traits for further analysis; lesion yellowness (the proportion of yellow pixels within the lesion to total pixels within the lesion), lesion greenness (total mm^2 of green pixels within the lesion), and lesion eccentricity (maximum lesion diameter – minimum diameter/maximum lesion diameter). These traits, along with lesion size, represent a broad sampling of the identified variation in the traits and provide a diverse array of measurable aspects of the *A. thaliana – B. cinerea* interaction.

From the HCA, lesion yellowness provides a trait that is distinct from lesion size suggesting that it may provide a highly unique measure of the interaction. We also focused on lesion greenness to increase our sampling within the hierarchical cluster space around lesion yellowness. Lesion greenness may be related to the presence of green islands that were noted in other plant pathogen interactions but have not been commonly studied (Walters et al., 2008). Lesion eccentricity was chosen as it is a spatial trait that is uncorrelated with lesion size traits. Previous work in our lab had suggested that lesion shape variation may be linked to genetic variation in the pathogens ability to identify and grow directionally along the mid-vein of the host leaf (Corwin et al., 2016a). Thus, including this trait may provide unique genetic insight into the ability of the pathogen to directionally orient growth along primary leaf vasculature within the host. We also included lesion size (mm^2) in our analysis to provide a direct comparison to previous reports. Thus, these four traits appear to have natural genetic variation both within the plant and pathogen that may provide unique insights into the plant/pathogen interaction.

Genetic Variation in New Lesion Traits

We utilized the phenotypic measurements for all four traits across all genotypic interactions of *A. thaliana* and *B. cinerea* to quantitatively assess the role of host and pathogen genetic variation in controlling these traits. We used linear models to analyze the variance across the 96 *A. thaliana* accessions and the four *B. cinerea* isolates. The genetic variation in both the pathogen and the host significantly influenced all four resistance associated traits (Table1). The proportion of variance attributable to *A. thaliana* accession was significant for these four traits, although relatively small for this experiment. The heritability across the entire dataset that was solely attributable to *A. thaliana* was relatively low albeit significant for each trait tested (Table 1). The proportion of heritability attributable to pathogen genetic variation was higher for the color and size traits ranging from 10-40% but there was no significant heritability within this small collection of isolates ascribed to pathogen variation for lesion eccentricity (Table 1). In contrast, the eccentricity was controlled by the interaction of genetic variation in the host and pathogen (Table 1), suggesting that this trait is highly dependent on the interaction between the pathogen genotypes and the different plant accessions. Thus, there is significant genetic variation for all traits that is dependent upon both the host and pathogen genomic diversity.

For further analysis, we obtained the model-corrected least squared means from these linear models to account for the environmental influence. This should help to focus the analysis on the genetic influence of the plant host in the downstream genetic mapping. Given the significance of the interaction between plant accession and pathogen isolate, we analyzed each lesion trait individually for each pathogen genotype across the diverse *A. thaliana* accessions as a separate trait to maximize our ability to identify causal loci.

Analysis of Covariance of Lesion Traits

To test how the lesion size, color, and shape traits may correlate across the different host/pathogen combinations, we conducted an ANCOVA (Analysis of CoVariance) comparing each pair of traits across the 96 diverse *A. thaliana* accessions for each of the four *B. cinerea* isolates (Figure 3). Significant correlations ($p < 0.05$) between the color and size, traits indicate that these three traits are generally related. Lesion yellowness and greenness show a positive correlation, both overall and within each *B. cinerea* isolate group, and this correlation is

239 statistically consistent between groups (Figure 3). In contrast, lesion color (both greenness and
240 yellowness) and size, display significant variation amongst the *B. cinerea* isolates for the
241 relationship with B05.10 and Supersteak isolates showing a negative correlation between lesion
242 yellowness and size while Apple517 and UKRazz show a neutral or slightly positive correlation
243 (Figure 3). In contrast to color and lesion size, eccentricity does not display uniform correlations
244 across all the isolates. Instead, the significant correlations are highly dependent on the
245 interaction with isolate (Figure 3). For example in eccentricity by lesion size, there is a strong
246 negative correlation in the *B. cinerea* isolates B05.10 and Supersteak, while only a very slight
247 positive correlation in Apple517 and UKRazz.
248 This suggests that while there is some common and some trait dependent genetic
249 variation in how *A. thaliana* responds to these diverse *B. cinerea* isolates using these lesion
250 traits. This analysis revealed that while there is some correlation between the four lesion traits,
251 the host and pathogen genotypes alter these relationships indicating that there is not a simple
252 mechanistic basis for these relationships. Further, the four lesion traits represent measures of
253 distinct and nuanced interactions between the plant and pathogen, and that the genes
254 associated with each trait likely influence different mechanisms in a multifaceted genetic
255 storyline.
256
257 **Genome-Wide Association Mapping of Lesion Traits**
258 To identify *A. thaliana* genes that are associated with these new lesion traits, we conducted a
259 genome-wide association (GWA) study. We used the model-corrected trait means for each *A.*
260 *thaliana* accession infected independently with the four different *B. cinerea* isolates across the
261 traits of lesion size, eccentricity (shape), and yellow and green color. We employed a publicly
262 available database of genomic polymorphisms across the 96 *A. thaliana* accessions consisting of
263 115,301 SNPs with minor allele frequency (MAF) of > 0.2 (Atwell et al., 2010; Corwin et al.,
264 2016b). The model for GWA mapping used a previously published ridge regression approach
265 with a permutated-effects threshold, which has previously been used to successfully identify
266 causal loci for both plant/pathogen interactions and plant metabolic variation (Shen et al.,
267 2013; Corwin et al., 2016b; Francisco et al., 2016; Kooke et al., 2016). Using the means for each

A. thaliana accession for each of the four lesion traits in response to the four individual *B. cinerea* isolates, we conducted GWA mapping for each combination separately for each isolate, resulting in four separate GWA maps for each trait. Because the variance and mean of each lesion phenotype differed according to pathogen genotype, the resulting effect sizes for *A. thaliana* SNPs also varied in magnitude. To create comparative Manhattan plots of the results for a single trait across all four *B. cinerea* isolates, we z-scaled the SNP effect sizes within each pathogen and overlaid the results (Figures 4 and 5). We calculated an effect size significance threshold for each individual trait by permuting the data one thousand times and running the ridge regression on the permuted data, and locating the 95th percentile (Tables S3-S6).

The comparative Manhattan plots (Figures 4, S2 and S3) showed that all four lesion associated traits lacked large, distinct SNP peaks. Instead, there are numerous significant SNPs with small-to-medium effect sizes distributed across the genome, suggesting a highly polygenic nature underlying the variation in these traits. Further, the significant SNPs different between the *B. cinerea* isolates, suggesting that most SNPs are dependent upon the interaction between plant and pathogen genotypes (Figures 4 and 5). For lesion Yellowness and Eccentricity, only Apple517 had significant SNPs possibly because this isolate had the highest level of phenotypic diversity in these traits (Figure 3). We next proceeded to identify putative causal loci in the GWA results by calling a gene as significantly associated with a trait if two or more SNPs within the coding region and 1 kb of the 5' upstream and 3' downstream regions had effect sizes above the 95th percentile threshold (Chan et al., 2011; Corwin et al., 2016b). This approach has previously been shown to reduce false positives within the dataset (Corwin et al., 2016b). Combining the analyses of each trait across the *B. cinerea* isolates for which there were significant SNPs identified 2,382 genes associate with lesion size, 4,383 with lesion yellowness, 4,110 with lesion greenness, and 1,933 with lesion eccentricity. Agreeing with the hypothesis that these traits can identify new cellular mechanisms, the majority of the genes identified are associated with only one or a few traits (Figure 5). Few genes (2.5% of 7940 total genes identified) were associated with all four lesion related traits (Figure 5). Of the genes associated with lesion size, 8% were not associated with any of the other three lesion traits. Likewise, 22% of genes associated with yellowness were associated exclusively with that phenotype, 20% for

297 green, and 7% for eccentricity. Overall, 57% of the genes found in this study associated with
298 only one of the lesion traits and 31% associate with exactly two of the lesion traits. These
299 results reinforce the idea that while there is some correlation between the traits, they are
300 quantitative traits that represent different measures of the plant-pathogen interaction.
301
302 **GO Category Enrichment Analysis**
303 We performed a gene ontology (GO) category enrichment analysis on biological processes of
304 genes associated with each of the four traits to identify *A. thaliana* mechanisms that may
305 influence variation in lesion traits. We performed GO enrichment analysis for each set of
306 candidate genes (Table 2). Both lesion color traits linked to genes involved in defense against
307 pathogens and insects (Table 2). They also identified unique enrichment categories wherein
308 each trait had different enriched categories. Specifically, lesion greenness shows enrichment in
309 maintenance of shoot apical meristem identity, and lesion yellowness in lignin biosynthetic
310 process. In contrast, eccentricity associated candidate genes are enriched in a variety of
311 unexpected processes, such as negative regulation of flower development and negative
312 regulation of reproductive process, in addition to known pathogen-associated processes, such
313 as cell wall thickening and callose deposition in cell walls. Genes controlling cell wall
314 modification play a role in plant defense strategies to contain the infected area, but have not
315 been studied in the context of lesion shape (Cantu et al., 2008; Mengiste et al., 2010; Bethke et
316 al., 2016). Thus, these novel visual traits are identifying known defense mechanisms while also
317 extending analysis out to new pathways.
318 In contrast to the individual trait candidate gene lists, The top enrichment categories for
319 the 200 *A. thaliana* genes that associate with all four lesion traits were defense response,
320 response to stress, immune response, plant-type hypersensitive response, programmed cell
321 death, chromatin remodeling, and response to salicylic acid (Table S2). Thus, the core genes
322 associated with all four lesion related traits linked in part to known defense genes. Overall, the
323 enrichment categories of genes associated with only a single trait uncovered several distinct
324 and unique biological processes that are tangentially associated with defense while genes
325 shared across four traits were more conservatively associated with defense. These differently

represented enrichment categories according to trait reflect varying, non-overlapping plant mechanisms involved in the multifaceted disease resistance against generalists. This analysis revealed four portraits of plant defense that showed some overlap but also revealed the extent of biochemical mechanisms involved in lesion traits.

Validation of Genes Associated with Lesion Phenotypes

To test whether the trait-associated genes we found in the GWA mapping were causal, we measured the infection-related phenotypes on knockout mutants of genes associated with each trait of interest. We chose 23 genes (Table 3) based on GWA effect-size ranking, specificity or overlap of traits effected, and ready availability of viable homozygous lines of T-DNA knockout mutants. The lines were grown, infected, and phenotyped using the same image analysis software as the initial 95 *A. thaliana* accessions. All mutants were tested for resistance against each isolate using 20 independent biological replicates per genotype spread across two experiments. All the traits were measured on each lesion and each trait was independently tested for a difference between WT and mutant using ANOVA (Table 3). The validation rate for lesion size was 60%, 33% for lesion yellowness, 38% for lesion greenness, and 20% for lesion eccentricity. Interestingly, this correlates with the overall fraction of each trait controlled by genetic variation (Table 1). This suggests that part of the lower validation rates for the new traits may be a power-to-detect effect issue and require increased replication. Another complication is that in our GWA mapping, we observed that effect sizes for individual SNPs within a single gene can be both positive and negative in comparison to the reference Col-0 accession (Figure 6 and Table 3). Thus, the natural loci likely have multiple haplotypes with differing functionalities while the validation mutants are unidirectional loss-of-function mutants within the reference Col-0 accession. We illustrate this with AT4G17010, a component of the transcription factor III B complex, where significantly associated SNPs have both positive and negative effects in comparison to the reference *A. thaliana* accession Col-0 (Figure 6 and Table 3). Three SNPs have effect sizes that fall above the 95th percentile threshold in the positive direction for lesion yellowness, and two have a similarly large magnitude in the negative

direction, indicating that the different haplotypes of this gene uniquely affect lesion yellowness (Figure 8). Clustering the accessions according to SNPs within this particular gene separates the haplotypes into five major groups, with groups I and II containing the SNPs with significant negative effect size, groups III and IV containing the SNP of greatest positive effect size, and group V containing the remaining diverse haplotypes (Figure 7). Even in the face of this complication, the T-DNA knockout mutant for the gene AT4G17010, did lead to altered lesion yellowness but not lesion size (Table 3). Thus, we can use GWA from high-throughput digital imaging to identify and validate new genes affecting visual lesion traits beyond lesion size.

Specific Loci and Trait Overlap

The validation tests showed that the genes were highly specific in their effects on the lesion traits by affecting only one or two traits. Only two genes, CESA2 and AT4G01883, were linked to three traits (Figure 8). Critically, no mutant affected all of the measured traits (Figure 7). This analysis identified new genes not previously linked to resistance to *B. cinerea*. A knockout mutant for *PHYTOCHROME E* (*phyE*), previously linked to shade avoidance, germination, seedling de-etiolation, and flowering time (Halliday and Whitelam, 2003), showed a statistically significant increase in lesion size and lesion yellowness compared to wildtype. It had been previously demonstrated that phyE affects stomatal conductance and photorespiration, which have been shown to play an important role in signaling programmed cell death and systemic acquired resistance defense response (Muhlenbock et al., 2008; Szechynska-Hebda et al., 2010). Other phytochromes, such as phyB, have been linked with defense response in *A. thaliana* via this pathway (Griebel and Zeier, 2008; Zhao et al., 2014) but there is no prior evidence in the literature of phyE affecting resistance. A knockout mutant of *SULFATE TRANSPORTER 4.1 (sultr4;1)* showed a greater lesion eccentricity. Sultr4;1 transports Sulphur from storage in the vacuole, facilitating the synthesis of Sulphur-containing amino acids and glutathione, a compound involved in balancing cellular redox (Zuber et al., 2010b). Sultr4;1 has not been previously linked with pathogen resistance, yet somehow plays a role in the defining the shape of a Botrytis lesion. This gene was neither associated with nor found to affect any of the other lesion traits, highlighting the importance of expanding the visual information used in

384 investigation of lesions. This highlights the utility of measuring different lesion related traits
385 beyond biomass or lesion size to identify new resistance mechanisms.
386
387 **Discussion**
388 In the analysis of plant/pathogen interactions, there is a dominant focus on measuring
389 pathogen success either as lesion area or pathogen biomass to quantify the level of
390 resistance/virulence in the interaction. However, this is merely one aspect of the interaction
391 and active infections can affect many different traits within the plant host (Agrios, 2005). New,
392 non-destructive imaging methods are beginning to illuminate other aspects of the host-
393 pathogen interaction that have largely been unstudied in mechanistic studies. Here, we utilized
394 a simple digital imaging platform to show that it is possible to identify the genetic basis of these
395 other defense-related traits, such as the color and shape of the developing lesion in addition to
396 the traditional size of the lesion. This shows that the generation of these visual traits is
397 genetically determined by variation in the host, the pathogen and the interaction of genetic
398 variation in the two organisms similarly to lesion size but can identify genes not known to
399 influence lesion size.
400 Conducting GWAS within the *A. thaliana* accessions and mutant validation studies
401 showed that these four traits had a blend of distinct and overlapping genetic mechanisms
402 controlling their generation. Classical *B. cinerea* resistance genes, like *COI1* and *PAD3*,
403 influenced both color and size of the developing lesion, but not the shape of the lesion,
404 showing the role of known resistance mechanisms in these new lesion traits (Thomma et al.,
405 1998; Ferrari et al., 2003; Kliebenstein et al., 2005; Rowe et al., 2010)(Figure 7). In contrast,
406 some known resistance genes like *ACD6* affected only the color but not the size or shape of the
407 lesion (Rate et al., 1999; Song et al., 2004; Lu et al., 2009)(Figure 7). More importantly, using
408 new lesion-related traits for GWAS identified new genes involved in resistance to *B. cinerea*
409 that had not previously been identified. This includes genes involved in light signal transduction,
410 LUX, PHOT1 and PHYE, as well as sulfur transport (Clack et al., 1994; Devlin et al., 1998; Briggs
411 and Christie, 2002; Halliday and Whitelam, 2003; Kataoka et al., 2004; Hazen et al., 2005; Zuber
412 et al., 2010a; Nusinow et al., 2011; Sanchez-Lamas et al., 2016). The three light-related genes

affected different lesion traits with PHOT1 being specific to lesion size, PHYE altering lesion size and yellowing while LUX and the sulfur transporter specifically altered lesion size (Figure 7). Thus, even these three genes that might have been expected to have overlapping effects show different and distinct effects from each other. This shows that there are specific mechanisms for each set of the traits and to fully understand the interaction requires more than simply measuring pathogen growth.

Lesion Eccentricity as an Indicator of Pathogen Success.

One difficulty of new traits from high-throughput digital imaging is to comprehend their possible biological role. For example lesion eccentricity (i.e. deviation from circularity) is a trait that is genetically controlled by both the pathogen and the host genes. Heritability of lesion eccentricity was 4.3% for plant accession, <0.1% for isolate, but jumped to 11.1% for accession:isolate, indicating that variation in this trait is highly dependent on the interaction of plant and pathogen genotypes. In two of the four pathogen genotypes, B05.10 and Supersteak, there was a negative correlation between lesion size and eccentricity suggesting that eccentric lesions tend to be smaller (Figure 3). In previous work, we had shown that eccentric lesions are associated with preferential growth along the primary vasculature, which implies that there is a shift from general radial outward growth to directed growth along the leaf midrib (Corwin et al., 2016a). Purely radial growth is typically considered to maximize local growth in microbial organisms and that would argue that directed growth may foresake potential local growth. A possible reason for forsaking local growth is that this could be a virulence strategy of some pathogen isolates to more rapidly move systemically through the vasculature of the plant. The fact that there are plant genes specific to affecting this trait indicates that *A. thaliana* has specific mechanisms that are geared towards altering the pattern of pathogen growth. As such, the success of the pathogen in the host-pathogen interaction would be a combination of the ability to infect the local tissue as well as move to distal tissue rapidly. Equally, if the pathogen has different growth strategies to optimize fitness, the plant would have to defend against local growth and growth geared towards spread of the pathogen.

Lesion Color Genetic Mechanisms and Agriculture

It is harder to assess the potential ecological or evolutionary role of specific genetic mechanisms influencing the color of a lesion. However, lesion color is a potentially key aspect of the plant-pathogen interaction for vegetable and fruit crops. For example, a very small lesion that gives rise to a highly noticable color (e.g. Figure 1c) on a fruit or vegetable would greatly decrease the consumer acceptance of that product and lead to post-harvest crop loss if the lesion was large. As such, understanding the specific genetic mechanisms influencing the different color traits can have significant agricultural importance and they are presently not studied. Our study showed that as previously described, COI1 plays a key role in controlling the development of yellow in the plant-pathogen interaction (Rowe et al., 2010). This agrees with the known connection of jasmonate signaling to photosynthetic/plastid functioning (Kazan and Manners, 2011; Attaran et al., 2014; Campos et al., 2016). Interestingly, this also showed that additional genes not previously known to affect *B. cinerea* resistance also function in determining the level of lesion yellowness, like PHYE (Figure 8).

Genes associated with lesion greenness were enriched in activation of the immune system, activation of the innate immune system, and movement of cellular or subcellular components. These biological processes have obvious roles in plant response to a fungal infection, but their links with lesion greenness are less obvious. Previous studies had identified green islands in some plant-pathogen interactions, dead green tissue within pathogen lesions, as associated with increased levels of cytokinins and polyamines that delay senescence, as well as a variety of fungal toxins (Walters et al., 2008). We previously attempted to extract green color from lesions using both methanol and hexane, but were unsuccessful, indicating that the source of this greenness is not free chlorophyll (Corwin et al., 2016a). Further, greener lesions had no living plant cells from what we could assess with trypan blue staining (Corwin et al., 2016a). However, the genes associated with greenness included known *B cinerea* resistance genes like COI1, PAD3 and PAD4 (Figure 7). Interestingly, the only gene solely associated with lesion greenness was ACD6, a gene that is key to regulating plant cell death in response to pathogen attack. This suggests that there may be a role for how the plant cell dies in controlling this color. While our results do not provide an immediate direct mechanism for the color traits,

it does show that there are potential mechanisms specific to the color traits in plant-pathogen interactions that maybe useful for understanding the infection process.

Conclusion

This study has utilized high-throughput digital imaging of plant-pathogen interactions to uncover the genetics for previously uncharacterized lesion traits. Many of the candidate genes that were tested with insertional mutants affected more than one aspect of the plant-pathogen interaction, color, lesion size or shape of the lesion. But no gene affected all of these aspects of the interaction. As most studies of quantitative resistance focus on biomass or lesion size measurements while not studying lesion shape or color, our findings suggest that there are potentially unrecognized mechanisms that may be important for plant-pathogen interactions. Further validation studies could reveal more large-effect plant genes affecting quantitative resistance, filling gaps in our knowledge of cellular mechanisms involved in lesion traits and pathogen virulence and deserving of attention in plant breeding programs. Equally, these traits raise the need for broader life-history studies of plant-pathogen interactions in the field to identify the potential ecological or evolutionary drivers of these traits. GWA mapping coupled with high-throughput digital measurement of virulence-associated traits will be a useful tool in understanding broader plant-pathogen interactions.

Materials & Methods

Population Selection for GWAS

We used a previously published collection of 96 *A. thaliana* accessions that was chosen for pathogen resistance GWAS based on similarity in flowering time (63.1 ± 0.95 (s.e.) days to flowering). This population minimizes the indirect effects of ontogenic variation caused by a wide range of flowering times, while also reducing the effect of rare, medium effect alleles in order to inflate genetically-related residuals (Corwin et al., 2016b). Selection based on flowering time also removed genetic outliers and minimized population structure. The selected population extends broadly across the known phylogeny of *A. thaliana* accessions, increasing the resolution of the association study (Corwin et al., 2016b).

500

501 **Growth Conditions and Pathogen Infection**

502 Seeds were cold stratified in 1% Phytagar at 4°C for seven days prior to sowing. Seeds were
503 then sown in a randomized complete block design with three seeds per cell, into four 104-cell
504 flats containing standard potting soil (Sunshine Mix #1, Sun Gro Horticulture, Agawam, MA).
505 Plants were covered with a transparent humidity dome, placed in short day (10h full spectrum
506 light) conditions in a controlled environment at 22°C, and watered biweekly as needed. After
507 one week, seedlings were thinned to one seedling per pot. Sowing was repeated two weeks
508 later to create another balanced randomized experiment so that eight biological replicates per
509 accession were present across the two independent experiments in a randomized complete
510 block design.

511 After five weeks of growth, mature leaves were excised, and placed on agar flats (Denby
512 et al., 2004; Rowe and Kliebenstein, 2008). Individual leaves were inoculated with either one of
513 four phenotypically and genotypically diverse isolates of *B cinerea* (Apple517, B05.10,
514 Supersteak, UKRazz) or a mock-inoculated control (Atwell et al., 2015; Corwin et al., 2016b;
515 Corwin et al., 2016a). Spores of five-day old sporulation cultures grown on organic peach slices
516 were collected in sterilized 1/2x organic grape juice, counted with a hemocytometer, and
517 standardized to a solution of 10 spores μl^{-1}. Individual leaves were inoculated with a single 4µl
518 droplet of one of the *B. cinerea* isolates or mock-inoculated with a control of 1/2x organic grape
519 juice, for approximately 40 spores per leaf. The inoculated leaves were kept under transparent
520 humidity domes at room temperature to allow lesions to grow for three days. At 72 hours post
521 inoculation (hpi), photos were taken of infected leaves along with a 1 cm^2 scale for size
522 reference using an 18 Megapixel high resolution T3i Canon camera outfitted with an EF-S 10-
523 22mm f/3.5–4.5 USM ultra-wide angle lens, achieving a resolution of approximately 10 pixels
524 per mm (Corwin et al., 2016b).

525

526 **Image Analysis**

527 A semi-automated image analysis script using the open-source R statistical environment (R
528 Development Core Team, 2016) and the Bioconductor packages EBImage and CRImage

(Failmezger H, 2010; Pau et al., 2010) was used to measure lesion traits such as lesion size, shape, and color (Corwin et al., 2016b). Briefly, the script identified leaves as objects that are have a green hue and highly saturated at their perimeter, whereas lesions were brown objects of low saturation within the leaf perimeter. Lesion and leaf mask images were generated and manually refined, or corrected where faulty. The area in pixels of these leaves and lesions, as well as the numbers and proportions of pixels of certain colors, and dimensions such as major and minor axes, perimeter, and eccentricity, were recorded. These values were converted to mm^2 using a 1 cm reference standard contained within each image.

Genome Wide Association Mapping

For each trait, we modeled heritability and obtained the model corrected least squared means using the linear model:

$$\text{Lesion trait}_{epab} \sim \beta 0 + E_e + P_p + A_a + B_b + A{:}B_{ab} + \varepsilon_{epab}$$

where E is experimental replicate, P is the individual plant, A is the genotype of the Arabidopsis accession and B is the genotype of the Botrytis isolate. Experimental replicate was modeled as a random effect, whereas individual plant, Arabidopsis accesion and Botrytis isolate were categorical. Publicly available data on genomic polymorphisms of the selected *A. thaliana* accessions was collected from the *A. thaliana* 1,001 genomes project (Ossowski et al., 2008; Cao et al., 2011; Gan et al., 2011; Schneeberger et al., 2011; Long et al., 2013; Alonso-Blanco et al., 2016). SNPs with minor allele frequency (MAF) < 0.2 were filtered out, resulting in a set of 115,310 SNPs for the 95 accessions. Association mapping was performed using the bigRR package in the R statistical environment (Shen et al., 2013). This previously published and validated method uses ridge regression, an appropriate approach given the small proportion of phenotypic variance attributable to genotype (Corwin et al., 2016b; Francisco et al., 2016). The ridge regression models the effects of all polymorphisms in a single model, treating each SNP as a random effect and introducing a bias to the regression estimates to reduce standard error. Thus, each polymorphism is assigned a heteroscedastic effect size (HEM), rather than a p-value, which is difficult to determine for random variables. Instead, a significant effect threshold value is delineated by permuting the phenotype data as it corresponds to the polymorphism data

1,000 times, and taking the 95th and the 99th percentiles. A gene is considered to be associated with a trait when two or more SNPs within the coding region have an effect size greater than the 95th percentile threshold. This is a functional genome wide prediction method that has been shown to provide similar results to EMMA based GWAS (Kooke et al., 2016). Further, this GWAS pipeline has yielded a high rate of gene validation for a number of traits within *A. thaliana* (Corwin et al., 2016b; Francisco et al., 2016).

GO Enrichment Analysis

Gene ontology (GO) enrichment analysis for biological processes was performed on all genes significantly associated with each of the four lesion traits using the Bioconductor packages org.At.tair.db, topGO, and goProfiles in the R statistical environment. Genes within *A. thaliana* that contain at least two significant SNPs that were associated with the trait of interest in the dataset were used as the genomic background sample for the analysis.

Validation Tests

A selection of 23 *A. thaliana* genes that were found to be highly associated with Lesion Size, Lesion Greenness, Lesion Yellowness, and Lesion Eccentricity was made based on ready availability of viable homozygous T-DNA knockout lines. Seventeen of the lines had been previously identified and tested for lesion size and an additional six genes were chosen based on the magnitude of predicted effect size (Corwin et al., 2016b). Plants were grown as described above and no genotypes showed any evidence of flowering within this time frame in these conditions. At five weeks of age, the six first fully mature leaves were excised and inoculated with the four isolates of *B. cinerea* mentioned above at the same concentrations, and imaged at 72 hpi. These leaves showed no visual evidence of senescence at the start of the experiment and the control grape juice mock-inoculated leaves showed no developing lesion during the image analysis. The experiment was carried out in a randomized complete block design, with two experimental replicates each containing 10 biological replicates, amounting to 20 replicates for each *A. thaliana* mutant / *B. cinerea* isolate combination. Statistical differences

between the WT Col-0 background and each mutant genotype were assessed using the linear model:

$$\text{Lesion trait}_{epi} \sim \beta 0 + E_e + P_p + I_i + P{:}I_{pi} + \varepsilon_{epi}$$

where E is experimental replicate, P is plant genotype, and I is the fungal isolate genotype. Experimental replicate was modeled as a random effect, where plant and fungal isolate genotypes were categorical.

Acknowledgments

Financial support for this work was provided by the National Research Foundation DNRF grant 99, US NSF grants IOS 1339125, MCB 1330337 and IOS1021861, and the USDA National Institute of Food and Agriculture, Hatch project number CA-D-PLS-7033-H.

TABLE 1 – Heritability of Lesion Traits

For each of the four traits, the table displays the sum of squares for each term in an analysis of variance, p values for each term, and the calculated heritability (proportion of total variance) attributed to the specific model terms. The analysis used the model Lesion Trait ~ Experiment + Accession * Isolate.

	SS	P	Heritability
Size			
Experiment	1224	0.002	
Plant	179962	< 0.001	
Accession	25273	< 0.001	3.0%
Isolate	333466	< 0.001	39.5%
Accession:Isolate	57552	< 0.001	6.8%
Yellow			
Experiment	2387113	0.036	
Plant	964232385	< 0.001	
Accession	70751623	0.014	2.5%
Isolate	557388090	< 0.001	20.0%
Accession:Isolate	176639269	0.083	6.3%
Green			
Experiment	3	0.281	
Plant	3958	< 0.001	
Accession	756	< 0.001	6.1%
Isolate	1232	< 0.001	10.0%
Accession:Isolate	1084	< 0.001	8.8%
Eccentricity			
Experiment	0.00070	0.842	
Plant	13.04996	0.003	
Accession	2.34077	0.008	4.3%
Isolate	0.00387	0.974	<0.1%
Accession:Isolate	6.00843	0.022	11.1%

615 **TABLE 2 – GO Categories enrichment**

616 The table displays the top ten enrichment categories (biological processes) associated with each
617 of the four lesion traits.

GO.ID	Term	p	Trait
GO:0006952	defense response	1.40E-05	Size
GO:1901264	carbohydrate derivative transport	0.0003	Size
GO:0009617	response to bacterium	0.0007	Size
GO:0006749	glutathione metabolic process	0.0027	Size
GO:0009556	microsporogenesis	0.0028	Size
GO:0006897	endocytosis	0.0043	Size
GO:0030029	actin filament-based process	0.0048	Size
GO:0048236	plant-type spore development	0.0050	Size
GO:0072523	purine-containing compound catabolic process	0.0061	Size
GO:1903409	reactive oxygen species biosynthetic process	0.0081	Size
GO:0009910	negative regulation of flower development	0.0011	Eccentricity
GO:2000242	negative regulation of reproductive process	0.0015	Eccentricity
GO:0006349	regulation of gene expression by genetic imprinting	0.0021	Eccentricity
GO:0071514	genetic imprinting	0.0021	Eccentricity
GO:0052386	cell wall thickening	0.0055	Eccentricity
GO:0052543	callose deposition in cell wall	0.0055	Eccentricity
GO:0009617	response to bacterium	0.0093	Eccentricity
GO:0010150	leaf senescence	0.0093	Eccentricity
GO:0006821	chloride transport	0.0107	Eccentricity
GO:0015700	arsenite transport	0.0107	Eccentricity
GO:0006952	defense response	0.0002	Green
GO:0010492	maintenance of shoot apical meristem identity	0.0046	Green
GO:0002218	activation of innate immune response	0.0051	Green
GO:0002253	activation of immune response	0.0051	Green
GO:0042742	defense response to bacterium	0.00520	Green
GO:0009617	response to bacterium	0.0068	Green
GO:0006928	movement of cell or subcellular component	0.0092	Green
GO:0030048	actin filament-based movement	0.0092	Green
GO:0034614	cellular response to reactive oxygen species	0.0093	Green
GO:0048236	plant-type spore development	0.0095	Green
GO:0006952	defense response	0.0002	Yellow
GO:0016568	chromatin modification	0.0011	Yellow
GO:0044699	single-organism process	0.0012	Yellow
GO:0009625	response to insect	0.0021	Yellow
GO:0044710	single-organism metabolic process	0.0022	Yellow
GO:0006325	chromatin organization	0.0029	Yellow
GO:0016569	covalent chromatin modification	0.0033	Yellow
GO:0009809	lignin biosynthetic process	0.0039	Yellow
GO:0042886	amide transport	0.0039	Yellow
GO:0006857	oligopeptide transport	0.0045	Yellow

618

TABLE 3. Candidate Gene Assessment

The table shows the validation tests on mutants in 23 potential candidate genes for each of the four measures of lesion formation: size, yellowness, greenness and eccentricity. The # of SNPs classified as significant above the 95 percentile threshold for that trait for that gene are shown as well as the significance of the difference between the insertion mutant and WT across all *B. cinerea* isolates (P – Plant) or an interaction with *B. cinerea* isolates (P – Plant:Isolate). Significance was tested using the models mentioned in the Method section. Nominal p-values between 0.1 and 0.05 are provided if at least one other trait showed significance below 0.05.

				Size			Yellow			Green			Eccentricity		
AGI	Gene	Mutant	#SNPs in coding region	# unique SNPs above 95	P - Plant	P - Plant: Isolate	# unique SNPs above 95	P - Plant	P - Plant: Isolate	# unique SNPs above 95	P - Plant	P - Plant: Isolate	# unique SNPs above 95	P - Plant	P - Plant: Isolate
AT2G25540	CESA10	cesA10-1	11	2	0.005	NS	4	0.053	NS	2	NS	NS	3	NS	NS
AT2G39940	COI1	coi1-1	4	0	< 0.001	0.096	4	< 0.001	NS	0	< 0.001	NS	0	NS	NS
AT1G01060	LHY	lhy-20	2	2	0.006	0.093	2	NS	NS	2	0.028	0.014	1	NS	NS
AT3G26830	PAD3	pad3-1	1	1	< 0.001	0.014	0	0.004	NS	0	0.008	0.069	0	NS	NS
AT3G52430	PAD4	pad4-1	6	0	0.002	0.062	0	NS	NS	1	0.010	0.019	4	NS	NS
AT4G39350	CESA2	CS818491	8	3	0.020	NS	2	NS	NS	2	0.067	NS	0	0.090	NS
AT1G22070	TGA3	tga3-2	1	0	NS	NS	0	NS	NS	0	NS	NS	1	NS	NS
AT4G17010	AT4G17010	CS861804	7	3	NS	NS	4	0.048	NS	2	NS	NS	1	0.020	NS
AT1G14690	MAP65	CS872894	10	0	NS	NS	0	NS	0.076	0	NS	NS	0	NS	NS
AT4G01883	-	CS67496	6	0	0.083	NS	0	NS	NS	2	0.056	NS	0	0.043	NS
AT4G14420	AT4G14420	N508498	6	2	0.046	NS	1	NS	NS	2	0.003	NS	2	NS	NS
AT4G14400	ACD6	N559132	20	3	NS	NS	5	NS	NS	15	0.047	NS	0	NS	NS
AT4G14368	-	N574598	16	3	NS	NS	0	NS	NS	6	NS	NS	0	NS	NS
AT1G31260	ZIP10	N604586	9	5	NS	NS	3	NS	NS	0	NS	NS	6	NS	NS
AT4G01860	-	N606172	13	1	NS	NS	0	NS	NS	6	NS	NS	0	NS	NS
AT2G32150	-	N640067	6	0	NS	NS	0	NS	NS	1	NS	NS	0	NS	NS
AT4G01880	-	CS857701 N608769	4	0	0.012	NS	1	0.037	NS	1	0.079	NS	0	NS	NS
AT3G46640	LUX	lux	5	0	NS	NS	0	NS	NS	4	NS	NS	0	0.046	NS
AT3G45780	PHOT1	phot1	6	3	NS	0.052	1	NS	NS	5	NS	NS	0	NS	NS
AT4G18130	PHYE	phyE-2	3	3	0.002	NS	0	0.024	NS	0	NS	NS	0	NS	NS
AT4G39030	SID1	sid1	9	0	NS	0.014	0	NS	NS	8	NS	NS	0	NS	NS
AT5G67370	CGLD27	N529971	4	0	NS	NS	3	NS	NS	1	NS	NS	0	NS	NS
AT5G45950	-	N582692	5	1	NS	NS	4	NS	NS	0	NS	NS	0	NS	NS
AT1G20910	-	N641443	5	0	NS	0.023	0	NS	NS	5	NS	NS	1	NS	NS
AT5G13550	SULTR4;1	N662135	5	0	NS	NS	0	NS	NS	0	NS	NS	5	0.094	NS

Figure Legends

FIGURE 1. Illustration of different lesion traits

The six *A. thaliana* leaves infected with *B cinerea* represent differing combinations of lesion traits observed. Lesions can be more circular or more eccentric, with pointed ends growing along the mid-vein of the leaf. Greenness and yellowness of both within the lesion and surrounding tissue is also highly variable. The water soaked greyish sectors represent the actual infected lesion.

a. Large eccentric lesion with enhanced senescence
b. Moderate eccentric lesion with low senescence
c. Small lesion with large senescence
d. Moderate circular lesion with moderate senescence
e. Small lesion with moderate senescence
f. Moderate circular lesion with large senescence

FIGURE 2. Hierarchical cluster analysis of lesion traits

The heat map shows the collection of 75 lesion measurements of the four *B. cinerea* isolates (columns) on the collection of 96 *A. thaliana* accessions (rows). Labeled lines show lesion size, yellowness, greenness and eccentricity for the *B. cinerea* BO5.10 isolate.

FIGURE 3. Isolate dependency of Ttait correlations across the isolates

ANCOVA was used to test for correlations between each pair of traits across the 96 *A. thaliana* isolates using each of the four different *B. cinerea* isolates. Scatter plots with 95% confidence interval for the trait correlation in each isolate are shown on the left half of the plot. The diagonal shows the distribution of the specific trait across the four *B. cinerea* isolates. The right hand tables show the p-values for the trait-trait correlations, *B. cinerea* isolate dependency of these correlations, and the interaction of *B. cinerea* isolate on the trait-trait correlation (Int) using the following model). The estimated slopes for each trait-trait interaction for each *B. cinerea* isolate are shown by the colored text.

FIGURE 4. Lesion size GWAS for four *B. cinerea* isolates

Manhattan plots showing lesion size trait GWAS results, as measured on four *B. cinerea* isolates: a, Apple517; b, B05.10; c, Supersteak; and d, UKRazz. The horizontal red-line shows the significance threshold as estimated by permutation.

FIGURE 5. Venn diagram of genes found in GWA mapping

A Venn diagram of the candidate *A. thaliana* genes found to associate with each lesion trait via GWA. The number of genes listed for each lesion trait reflects the number of genes with two or more SNPs above the 95^{th} percentile threshold for that particular trait.

FIGURE 6. Haplotype diversity effects on trait to genotype linkages using AT4G17010

a) Plot of z-scaled SNP effect size across all four *B. cinerea* isolates on lesion yellowness within 1000bp of the AT4G17010 coding region (represented in blue bocks) of AT4G17010. The arrow indicates the transcriptional start site. The horizontal orange lines indicate the positive and

negative permutation thresholds for the *B. cinerea* isolate Apple517. The letters show the SNPs that are significantly associated with lesion yellowness in *B. cinerea* Apple517.
b) Hierarchical clustering of 95 *A. thaliana* accessions based on SNPs within AT4G17010. Haplotypes are assigned into five major groups, denoted by Roman numerals. Light grey indicates the SNP is the Col-0 allele while dark grey is the opposite allele. The SNPs are presented in their genomic order rather than the haplotype grouped structure.
c) Distributions of lesion yellowness across the *A. thaliana* accessions infected with *B. cinerea* Apple517. The *A. thaliana* accessions are grouped by approximate SNP haplotypes in b. The model corrected mean value of lesion yellowness for *A. thaliana* reference accession Col-0 was 0.545. Significance differences between the groups are shown by letters.

FIGURE 7 – Lesion traits affected by T-DNA insertional mutants
A Venn diagram showing the lesion traits significantly affected by each of the T-DNA knockout mutants in comparison to the wildtype background. The gene identifiers are located within the appropriate section of the diagram showing all the phenotypes altered by mutations in that gene.

Supplemental Materials

Figure S1: Hierarchical Cluster Analysis of Lesion Traits
Hierarchical cluster analysis of the a) four traits chosen to represent broad visual aspects of lesions, across the four pathogen isolates. b) Detail showing only color and shape traits illustrates relatedness and variation across accessions and isolates.

Figure S2: Lesion Greenness Manhattan Plots
Manhattan plots showing lesion greenness trait GWAS results, as measured on four *B. cinerea* isolates: a, Apple517; b, B05.10; c, Supersteak; and d, UKRazz. The horizontal red-line shows the significance threshold as estimated by permutation.

Figure S3: Lesion Yellowness and Eccentricity Shape Manhattan Plots for Apple517
Manhattan plots showing lesion yellowness (a) and eccentricity trait (b) GWAS results for Apple517. There were no significant SNPs identified for the other isolates. The horizontal red-line shows the significance threshold as estimated by permutation.

Table S1. LSMeans for all measured lesion traits. The model corrected mean value for all 75 measures lesion traits across all accessions for all isolates.

Table S2. GO Enrichment Test using the 200 candidate genes associated with all four lesion Traits. Annotated shows the total number of genes in the genome for the given term. Significant shows the number of candidate genes with this term and Expected is the number expected by random chance. Classic Fisher is the p-value for enrichment of this term.

Table S3. Lesion Area GWA

Presented are the estimated effect sizes for all SNPs using lesion area for each isolate. The absolute value of the permutation estimated effect size are shown to the right for each isolate.

Table S4. Lesion Greenness GWA
Presented are the estimated effect sizes for all SNPs using lesion greenness for each isolate. The absolute value of the permutation estimated effect size are shown to the right for each isolate.

Table S5. Lesion Yellowness GWA
Presented are the estimated effect sizes for all SNPs using lesion yellowness for each isolate. The absolute value of the permutation estimated effect size are shown to the right for each isolate.

Table S6. Lesion Eccentricity GWA
Presented are the estimated effect sizes for all SNPs using lesion eccentricity for each isolate. The absolute value of the permutation estimated effect size are shown to the right for each isolate.

References

Agrios, G. (2005). Plant Pathology. (Elsevier Academic Press).

Aguileta, G., Lengelle, J., Chiapello, H., Giraud, T., Viaud, M., Fournier, E., Rodolphe, F., Marthey, S., Ducasse, A., Gendrault, A., Poulain, J., Wincker, P., and Gout, L. (2012). Genes under positive selection in a model plant pathogenic fungus, Botrytis. Infection Genetics and Evolution **12,** 987-996.

Alfonso, C., Raposo, R., and Melgarejo, P. (2000). Genetic diversity in Botrytis cinerea populations on vegetable crops in greenhouses in south-eastern Spain. Plant Pathology **49,** 243-251.

Alonso-Blanco, C., Andrade, J., Becker, C., Bemm, F., Bergelson, J., Borgwardt, K.M., Cao, J., Chae, E., Dezwaan, T.M., Ding, W., Ecker, J.R., Exposito-Alonso, M., Farlow, A., Fitz, J., Gan, X.C., Grimm, D.G., Hancock, A.M., Henz, S.R., Holm, S., Horton, M., Jarsulic, M., Kerstetter, R.A., Korte, A., Korte, P., Lanz, C., Lee, C.R., Meng, D.Z., Michael, T.P., Mott, R., Muliyati, N.W., Nagele, T., Nagler, M., Nizhynska, V., Nordborg, M., Novikova, P.Y., Pico, F.X., Platzer, A., Rabanal, F.A., Rodriguez, A., Rowan, B.A., Salome, P.A., Schmid, K.J., Schmitz, R.J., Seren, U., Sperone, F.G., Sudkamp, M., Svardal, H., Tanzer, M.M., Todd, D., Volchenboum, S.L., Wang, C.M., Wang, G., Wang, X., Weckwerth, W., Weigel, D., Zhou, X.F., and Genomes, C. (2016). 1,135 Genomes Reveal the Global Pattern of Polymorphism in Arabidopsis thaliana. Cell **166,** 481-491.

Amselem, J., Cuomo, C.A., van Kan, J.A.L., Viaud, M., Benito, E.P., Couloux, A., Coutinho, P.M., de Vries, R.P., Dyer, P.S., Fillinger, S., Fournier, E., Gout, L., Hahn, M., Kohn, L.M., Lapalu, N., Plummer, K.M., Pradier, J.M., Quevillon, E., Sharon, A., Simon, A., ten Have, A., Tudzynski, B., Tudzynski, P., Wincker, P., Andrew, M., Anthouard, V., Beever, R.E., Beffa, R., Benoit, I., Bouzid, O., Brault, B., Chen, Z.H., Choquer, M., Collemare, J., Cotton, P., Danchin, E.G., Da Silva, C., Gautier, A., Giraud, C., Giraud, T., Gonzalez, C., Grossetete, S., Guldener, U., Henrissat, B., Howlett, B.J., Kodira, C., Kretschmer, M., Lappartient, A., Leroch, M., Levis, C., Mauceli, E., Neuveglise, C., Oeser, B., Pearson, M., Poulain, J., Poussereau, N., Quesneville, H., Rascle, C., Schumacher, J., Segurens, B., Sexton, A., Silva, E., Sirven, C., Soanes, D.M., Talbot, N.J., Templeton, M., Yandava, C., Yarden, O., Zeng, Q.D., Rollins, J.A., Lebrun, M.H., and Dickman, M. (2011). Genomic Analysis of the Necrotrophic Fungal Pathogens Sclerotinia sclerotiorum and Botrytis cinerea. Plos Genetics **7**.

Attaran, E., Major, I.T., Cruz, J.A., Rosa, B.A., Koo, A.J.K., Chen, J., Kramer, D.M., He, S.Y., and Howe, G.A. (2014). Temporal Dynamics of Growth and Photosynthesis Suppression in Response to Jasmonate Signaling. Plant physiology **165,** 1302-1314.

Atwell, S., Corwin, J.A., Soltis, N.E., Subedy, A., Denby, K.J., and Kliebenstein, D.J. (2015). Whole genome resequencing of Botrytis cinerea isolates identifies high levels of standing diversity. Frontiers in Microbiology **6**.

Atwell, S., Huang, Y., Vilhjalmsson, B.J., Willems, G., Horton, M., Li, Y., Meng, D., Platt, A., Tarone, A., Hu, T.T., Jiang, R., Muliyati, N.W., Zhang, X., Ali Amer, M., Baxter, I.R., Brachi, B., Chory, J., Dean, C., Debieu, M., de Meaux, J., Ecker, J.R., Faure, n., Kniskern, J.M., Jones, J.D.G., Michael, T.P., Nemri, A., Roux, F., Salt, D.E., Tang, C.L., Todesco, M., Traw, M.B., Weigel, D., Marjoram, P., Borevitz, J.O., Bergelson, J., and Nordborg, M.

(2010). Genome-wide association study of 107 phenotypes in a common set of *Arabidopsis thaliana* in-bred lines. Nature **465,** 627-631.

Barbedo, J.G.A. (2017). A new automatic method for disease symptom segmentation in digital photographs of plant leaves. European Journal of Plant Pathology **147,** 349-364.

Bethke, G., Thao, A., Xiong, G.Y., Li, B.H., Soltis, N.E., Hatsugai, N., Hillmer, R.A., Katagiri, F., Kliebenstein, D.J., Pauly, M., and Glazebrook, J. (2016). Pectin Biosynthesis Is Critical for Cell Wall Integrity and Immunity in Arabidopsis thaliana. Plant Cell **28,** 537-556.

Bock, C.H., Poole, G.H., Parker, P.E., and Gottwald, T.R. (2010). Plant Disease Severity Estimated Visually, by Digital Photography and Image Analysis, and by Hyperspectral Imaging. Critical Reviews in Plant Sciences **29,** 59-107.

Briggs, W.R., and Christie, J.M. (2002). Phototropins 1 and 2: versatile plant blue-light receptors. Trends in plant science **7,** 204-210.

Campos, M.L., Yoshida, Y., Major, I.T., Ferreira, D.D., Weraduwage, S.M., Froehlich, J.E., Johnson, B.F., Kramer, D.M., Jander, G., Sharkey, T.D., and Howe, G.A. (2016). Rewiring of jasmonate and phytochrome B signalling uncouples plant growth-defense tradeoffs. Nature Communications **7**.

Cantu, D., Vicente, A.R., Greve, L.C., Dewey, F.M., Bennett, A.B., Labavitch, J.M., and Powell, A.L.T. (2008). The intersection between cell wall disassembly, ripening, and fruit susceptibility to Botrytis cinerea. Proceedings of the National Academy of Sciences of the United States of America **105,** 859-864.

Cao, J., Schneeberger, K., Ossowski, S., Gunther, T., Bender, S., Fitz, J., Koenig, D., Lanz, C., Stegle, O., Lippert, C., Wang, X., Ott, F., Muller, J., Alonso-Blanco, C., Borgwardt, K., Schmid, K.J., and Weigel, D. (2011). Whole-genome sequencing of multiple Arabidopsis thaliana populations. Nat Genet **43,** 956-U960.

Chan, E.K.F., Rowe, H.C., Corwin, J.A., Joseph, B., and Kliebenstein, D.J. (2011). Combining Genome-Wide Association Mapping and Transcriptional Networks to Identify Novel Genes Controlling Glucosinolates in Arabidopsis thaliana. Plos Biol **9**.

Choquer, M., Fournier, E., Kunz, C., Levis, C., Pradier, J.M., Simon, A., and Viaud, M. (2007). Botrytis cinerea virulence factors: new insights into a necrotrophic and polyphageous pathogen. Fems Microbiology Letters **277,** 1-10.

Clack, T., Mathews, S., and Sharrock, R.A. (1994). THE PHYTOCHROME APOPROTEIN FAMILY IN ARABIDOPSIS IS ENCODED BY 5 GENES - THE SEQUENCES AND EXPRESSION OF PHYD AND PHYE. Plant molecular biology **25,** 413-427.

Corwin, J.A., and Kliebenstein, D.J. (2017). Quantitative Resistance: More Than Just Perception of a Pathogen. Plant Cell **29,** 655-665.

Corwin, J.A., Subedy, A., Eshbaugh, R., and Kliebenstein, D.J. (2016a). Expansive Phenotypic Landscape of Botrytis cinerea Shows Differential Contribution of Genetic Diversity and Plasticity. Molecular Plant-Microbe Interactions **29,** 287-298.

Corwin, J.A., Copeland, D., Feusier, J., Subedy, A., Eshbaugh, R., Palmer, C., Maloof, J., and Kliebenstein, D.J. (2016b). The Quantitative Basis of the Arabidopsis Innate Immune System to Endemic Pathogens Depends on Pathogen Genetics. Plos Genetics **12**.

Denby, K.J., Kumar, P., and Kliebenstein, D.J. (2004). Identification of Botrytis cinerea susceptibility loci in Arabidopsis thaliana. Plant J **38,** 473-486.

Devlin, P.F., Patel, S.R., and Whitelam, G.C. (1998). Phytochrome E influences internode elongation and flowering time in Arabidopsis. Plant Cell **10,** 1479-1487.

Elad, Y., Pertot, I., Cotes Prado, A.M., and Stewart, A. (2016). Plant Hosts of Botrytis spp. In Botrytis – the Fungus, the Pathogen and its Management in Agricultural Systems, S. Fillinger and Y. Elad, eds (Cham: Springer International Publishing), pp. 413-486.

Failmezger H, Y.Y., Rueda O, Markowetz F. (2010). CRImage: CRImage a package to classify cells and calculate tumour cellularity.

Ferrari, S., Vairo, D., Ausubel, F.M., Cervone, F., and De Lorenzo, G. (2003). Tandemly duplicated Arabidopsis genes that encode polygalacturonase-inhibiting proteins are regulated coordinately by different signal transduction pathways in response to fungal infection. Plant Cell **15,** 93-106.

Francisco, M., Joseph, B., Caligagan, H., Li, B.H., Corwin, J.A., Lin, C., Kerwin, R.E., Burow, M., and Kliebenstein, D.J. (2016). Genome Wide Association Mapping in Arabidopsis thaliana Identifies Novel Genes Involved in Linking Allyl Glucosinolate to Altered Biomass and Defense. Frontiers in Plant Science **7**.

Gan, X.C., Stegle, O., Behr, J., Steffen, J.G., Drewe, P., Hildebrand, K.L., Lyngsoe, R., Schultheiss, S.J., Osborne, E.J., Sreedharan, V.T., Kahles, A., Bohnert, R., Jean, G., Derwent, P., Kersey, P., Belfield, E.J., Harberd, N.P., Kemen, E., Toomajian, C., Kover, P.X., Clark, R.M., Ratsch, G., and Mott, R. (2011). Multiple reference genomes and transcriptomes for Arabidopsis thaliana. Nature **477,** 419-423.

Giraud, T., Fortini, D., Levis, C., Leroux, P., and Brygoo, Y. (1997). RFLP markers show genetic recombination in Botryotinia fuckeliana (Botrytis cinerea) and transposable elements reveal two sympatric species. Molecular Biology and Evolution **14,** 1177-1185.

Griebel, T., and Zeier, J. (2008). Light regulation and daytime dependency of inducible plant defenses in arabidopsis: Phytochrome signaling controls systemic acquired resistance rather than local defense. Plant physiology **147,** 790-801.

Halliday, K.J., and Whitelam, G.C. (2003). Changes in photoperiod or temperature alter the functional relationships between phytochromes and reveal roles for phyD and phyE. Plant physiology **131,** 1913-1920.

Hazen, S.P., Schultz, T.F., Pruneda-Paz, J.L., Borevitz, J.O., Ecker, J.R., and Kay, S.A. (2005). LUX ARRHYTHMO encodes a Myb domain protein essential for circadian rhythms. Proceedings of the National Academy of Sciences of the United States of America **102,** 10387-10392.

Jarvis, W.R. (1977). Botryotinia and Botrytis species : taxonomy, physiology, and pathogenicity : a guide to the literature. (Ottawa: Research Branch, Canada Dept. of Agriculture: obtainable from Information Division, Canada Dept. of Agriculture).

Jones, J.D.G., and Dangl, J.L. (2006). The plant immune system. Nature **444,** 323-329.

Kataoka, T., Watanabe-Takahashi, A., Hayashi, N., Ohnishi, M., Mimura, T., Buchner, P., Hawkesford, M.J., Yamaya, T., and Takahashi, H. (2004). Vacuolar sulfate transporters are essential determinants controlling internal distribution of sulfate in Arabidopsis. Plant Cell **16,** 2693-2704.

Kazan, K., and Manners, J.M. (2011). The interplay between light and jasmonate signalling during defence and development. Journal of Experimental Botany **62,** 4087-4100.

Kliebenstein, D.J., Rowe, H.C., and Denby, K.J. (2005). Secondary metabolites influence Arabidopsis/Botrytis interactions: variation in host production and pathogen sensitivity. Plant Journal **44,** 25-36.

Kooke, R., Kruijer, W., Bours, R., Becker, F., Kuhn, A., van de Geest, H., Buntjer, J., Doeswijk, T., Guerra, J., Bouwmeester, H., Vreugdenhil, D., and Keurentjes, J.J.B. (2016). Genome-Wide Association Mapping and Genomic Prediction Elucidate the Genetic Architecture of Morphological Traits in Arabidopsis. Plant physiology **170,** 2187-2203.

Kretschmer, M., Leroch, M., Mosbach, A., Walker, A.-S., Fillinger, S., Mernke, D., Schoonbeek, H.-J., Pradier, J.-M., Leroux, P., De Waard, M.A., and Hahn, M. (2009). Fungicide-Driven Evolution and Molecular Basis of Multidrug Resistance in Field Populations of the Grey Mould Fungus Botrytis cinerea. Plos Pathogens **5**.

Kuska, M., Wahabzada, M., Leucker, M., Dehne, H.W., Kersting, K., Oerke, E.C., Steiner, U., and Mahlein, A.K. (2015). Hyperspectral phenotyping on the microscopic scale: towards automated characterization of plant-pathogen interactions. Plant methods **11**.

Laluk, K., and Mengiste, T. (2010). Necrotroph attacks on plants: wanton destruction or covert extortion? The Arabidopsis book / American Society of Plant Biologists **8,** e0136.

Leucker, M., Mahlein, A.K., Steiner, U., and Oerke, E.C. (2016). Improvement of Lesion Phenotyping in Cercospora beticola-Sugar Beet Interaction by Hyperspectral Imaging. Phytopathology **106,** 177-184.

Li, B., Hulin, M.T., Brain, P., Mansfield, J.W., Jackson, R.W., and Harrison, R.J. (2015). Rapid, automated detection of stem canker symptoms in woody perennials using artificial neural network analysis. Plant Methods **11**.

Long, Q., Rabanal, F.A., Meng, D.Z., Huber, C.D., Farlow, A., Platzer, A., Zhang, Q.R., Vilhjalmsson, B.J., Korte, A., Nizhynska, V., Voronin, V., Korte, P., Sedman, L., Mandakova, T., Lysak, M.A., Seren, U., Hellmann, I., and Nordborg, M. (2013). Massive genomic variation and strong selection in Arabidopsis thaliana lines from Sweden. Nat Genet **45,** 884-U218.

Lu, H., Salimian, S., Gamelin, E., Wang, G.Y., Fedorowski, J., LaCourse, W., and Greenberg, J.T. (2009). Genetic analysis of acd6-1 reveals complex defense networks and leads to identification of novel defense genes in Arabidopsis. Plant Journal **58,** 401-412.

Mahlein, A.K., Steiner, U., Hillnhutter, C., Dehne, H.W., and Oerke, E.C. (2012). Hyperspectral imaging for small-scale analysis of symptoms caused by different sugar beet diseases. Plant Methods **8**.

Matsunaga, T.M., Ogawa, D., Taguchi-Shiobara, F., Ishimoto, M., Matsunaga, S., and Habu, Y. (2017). Direct quantitative evaluation of disease symptoms on living plant leaves growing under natural light. Breeding Science **67,** 316-319.

Mengiste, T., Laluk, K., and AbuQamar, S. (2010). Mechanisms of Induced Resistance Against B. cinerea. Plant Path 21st**,** 13-30.

Montes, J.M., Melchinger, A.E., and Reif, J.C. (2007). Novel throughput phenotyping platforms in plant genetic studies. Trends in plant science **12,** 433-436.

Muhlenbock, P., Szechynska-Hebda, M., Plaszczyca, M., Baudo, M., Mateo, A., Mullineaux, P.M., Parker, J.E., Karpinska, B., and Karpinski, S. (2008). Chloroplast Signaling and LESION SIMULATING DISEASE1 Regulate Crosstalk between Light Acclimation and Immunity in Arabidopsis. (vol 20, pg 2339, 2008). Plant Cell **20,** 3480-3480.

Mutka, A.M., and Bart, R.S. (2015). Image-based phenotyping of plant disease symptoms. Front Plant Sci **5**.

Nusinow, D.A., Helfer, A., Hamilton, E.E., King, J.J., Imaizumi, T., Schultz, T.F., Farre, E.M., and Kay, S.A. (2011). The ELF4-ELF3-LUX complex links the circadian clock to diurnal control of hypocotyl growth. Nature **475,** 398-U161.

Ossowski, S., Schneeberger, K., Clark, R.M., Lanz, C., Warthmann, N., and Weigel, D. (2008). Sequencing of natural strains of Arabidopsis thaliana with short reads. Genome Res **18,** 2024-2033.

Pau, G., Fuchs, F., Sklyar, O., Boutros, M., and Huber, W. (2010). EBImage-an R package for image processing with applications to cellular phenotypes. Bioinformatics **26,** 979-981.

R Development Core Team. (2016). R: A Language and Environment for Statistical Computing (Vienna, Austria: R Foundation for Statistical Computing).

Rate, D.N., Cuenca, J.V., Bowman, G.R., Guttman, D.S., and Greenberg, J.T. (1999). The Gain-of-Function Arabidopsis acd6 Mutant Reveals Novel Regulation and Function of the Salicylic Acid Signaling Pathway in Controlling Cell Death, Defenses, and Cell Growth. Plant Cell **11,** 1695-1708.

Rowe, H.C., and Kliebenstein, D.J. (2008). Complex genetics control natural variation in *Arabidopsis thaliana* resistance to *Botrytis cinerea*. Genetics **180,** 2237-2250.

Rowe, H.C., and Kliebenstein, D.J. (2010). All Mold Is Not Alike: The Importance of Intraspecific Diversity in Necrotrophic Plant Pathogens. Plos Pathog **6**.

Rowe, H.C., Walley, J.W., Corwin, J., Chan, E.K.-F., Dehesh, K., and Kliebenstein, D.J. (2010). Deficiencies in jasmonate-mediated plant defense reveal quantitative variation in *Botrytis cinerea* pathogenesis. PLoS Pathogens **6,** e1000861.

Sanchez-Lamas, M., Lorenzo, C.D., and Cerdan, P.D. (2016). Bottom-up Assembly of the Phytochrome Network. Plos Genetics **12**.

Schneeberger, K., Ossowski, S., Ott, F., Klein, J.D., Wang, X., Lanz, C., Smith, L.M., Cao, J., Fitz, J., Warthmann, N., Henz, S.R., Huson, D.H., and Weigel, D. (2011). Reference-guided assembly of four diverse Arabidopsis thaliana genomes. Proceedings of the National Academy of Sciences of the United States of America **108,** 10249-10254.

Schwanck, A.A., and Del Ponte, E.M. (2016). Measuring lesion attributes and analysing their spatial patterns at the leaf scale using digital image analysis. Plant Pathology **65,** 1498-1508.

Shen, X., Alam, M., Fikse, F., and Ronnegard, L. (2013). A Novel Generalized Ridge Regression Method for Quantitative Genetics. Genetics **193,** 1255-1268.

Song, J.T., Lu, H., McDowell, J.M., and Greenberg, J.T. (2004). A key role for ALD1 in activation of local and systemic defenses in Arabidopsis. Plant Journal **40,** 200-212.

Staats, M., van Baarlen, P., and van Kan, J.A.L. (2005). Molecular phylogeny of the plant pathogenic genus Botrytis and the evolution of host specificity. Molecular Biology and Evolution **22,** 333-346.

Stefanato, F.L., Abou-Mansour, E., Buchala, A., Kretschmer, M., Mosbach, A., Hahn, M., Bochet, C.G., Metraux, J.P., and Schoonbeek, H.J. (2009). The ABC transporter BcatrB from Botrytis cinerea exports camalexin and is a virulence factor on Arabidopsis thaliana. Plant Journal **58,** 499-510.

Szechynska-Hebda, M., Kruk, J., Gorecka, M., Karpinska, B., and Karpinski, S. (2010). Evidence for Light Wavelength-Specific Photoelectrophysiological Signaling and Memory of Excess Light Episodes in Arabidopsis. Plant Cell **22,** 2201-2218.

Thomma, B., Eggermont, K., Penninckx, I., Mauch-Mani, B., Vogelsang, R., Cammue, B.P.A., and Broekaert, W.F. (1998). Separate jasmonate-dependent and salicylate-dependent defense-response pathways in Arabidopsis are essential for resistance to distinct microbial pathogens. Proc Natl Acad Sci U S A **95,** 15107-15111.

Thomma, B.P.H.J., Eggermont, K., Tierens, K.F.M.J., and Broekaert, W.F. (1999). Requirement of functional ethylene-insensitive 2 gene for efficient resistance of Arabidopsis to infection by Botrytis cinerea. Plant Physiol **121,** 1093-1101.

Vaczy, K.Z., Sandor, E., Karaffa, L., Fekete, E., Fekete, E., Arnyasi, M., Czegledi, L., Kovics, G.J., Druzhinina, I.S., and Kubicek, C.P. (2008). Sexual Recombination in the Botrytis cinerea Populations in Hungarian Vineyards. Phytopathology **98,** 1312-1319.

Valiuskaite, A., Surviliene, E., and Baniulis, D. (2010). Genetic diversity and pathogenicity traits of Botrytis spp. isolated from horticultural hosts. Zemdirbyste **97,** 85-90.

Veronese, P., Nakagami, H., Bluhm, B., AbuQamar, S., Chen, X., Salmeron, J., Dietrich, R.A., Hirt, H., and Mengiste, T. (2006). The membrane-anchored BOTRYTIS-INDUCED KINASE1 plays distinct roles in Arabidopsis resistance to necrotrophic and biotrophic pathogens. Plant Cell **18,** 257-273.

Walters, D.R., McRoberts, N., and Fitt, B.D. (2008). Are green islands red herrings? Significance of green islands in plant interactions with pathogens and pests. Biol Rev Camb Philos Soc **83,** 79-102.

Windram, O., Madhou, P., McHattie, S., Hill, C., Hickman, R., Cooke, E., Jenkins, D.J., Penfold, C.A., Baxter, L., Breeze, E., Kiddle, S.J., Rhodes, J., Atwell, S., Kliebenstein, D.J., Kim, Y.S., Stegle, O., Borgwardt, K., Zhang, C.J., Tabrett, A., Legaie, R., Moore, J., Finkenstadt, B., Wild, D.L., Mead, A., Rand, D., Beynon, J., Ott, S., Buchanan-Wollaston, V., and Denby, K.J. (2012). Arabidopsis Defense against Botrytis cinerea: Chronology and Regulation Deciphered by High-Resolution Temporal Transcriptomic Analysis. Plant Cell **24,** 3530-3557.

Zhao, Y.Y., Zhou, J., and Xing, D. (2014). Phytochrome B-mediated activation of lipoxygenase modulates an excess red light-induced defence response in Arabidopsis. J Exp Bot **65,** 4907-4918.

Zuber, H., Davidian, J.C., Wirtz, M., Hell, R., Belghazi, M., Thompson, R., and Gallardo, K. (2010a). Sultra4;1 mutant seeds of Arabidopsis have an enhanced sulphate content and modified proteome suggesting metabolic adaptations to altered sulphate compartmentalization. Bmc Plant Biology **10**.

Zuber, H., Davidian, J.C., Wirtz, M., Hell, R., Belghazi, M., Thompson, R., and Gallardo, K. (2010b). Sultr4;1 mutant seeds of Arabidopsis have an enhanced sulphate content and modified proteome suggesting metabolic adaptations to altered sulphate compartmentalization. BMC Plant Biol **10,** 78.

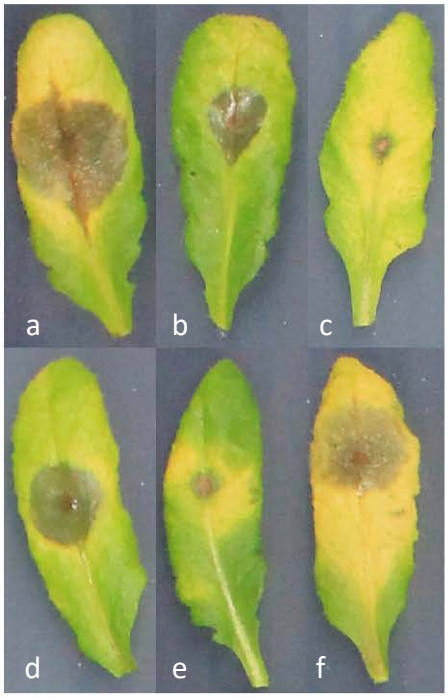

FIGURE 1. Illustration of different lesion traits

The six *A. thaliana* leaves infected with *B cinerea* represent differing combinations of lesion traits observed. Lesions can be more circular or more eccentric, with pointed ends growing along the mid-vein of the leaf. Greenness and yellowness of both within the lesion and surrounding tissue is also highly variable. The water soaked greyish sectors represent the actual infected lesion.

a. Large eccentric lesion with enhanced senescence
b. Moderate eccentric lesion with low senescence
c. Small lesion with large senescence
d. Moderate circular lesion with moderate senescence
e. Small lesion with moderate senescence
f. Moderate circular lesion with large senescence

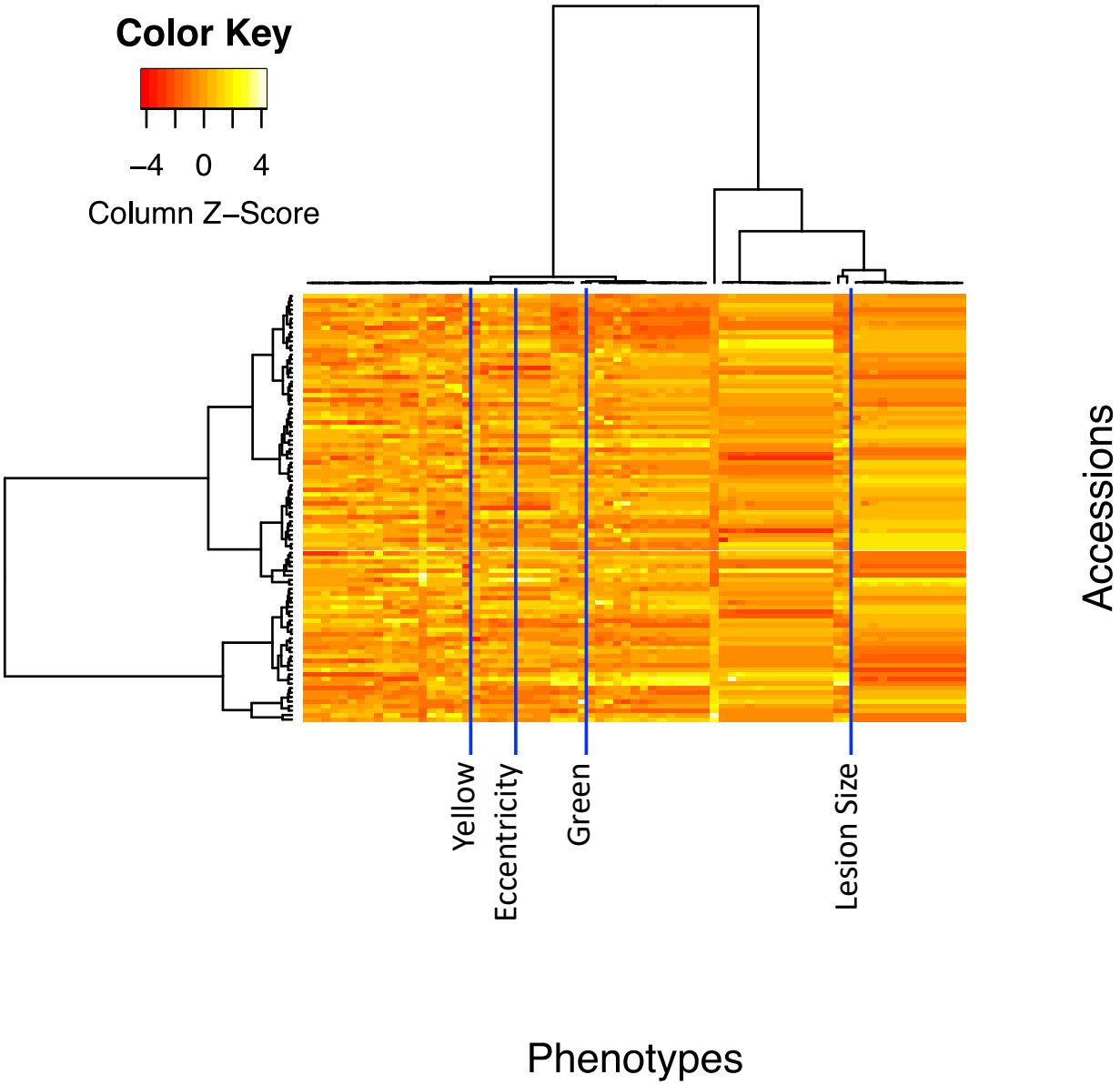

FIGURE 2 – Hierarchical cluster analysis of lesion traits

The heat map shows the collection of 75 lesion measurements of the four *B. cinerea* isolates (columns) on the collection of 96 *A. thaliana* accessions (rows). Labeled lines show lesion size, yellowness, greenness and eccentricity for the *B. cinerea* BO5.10 isolate.

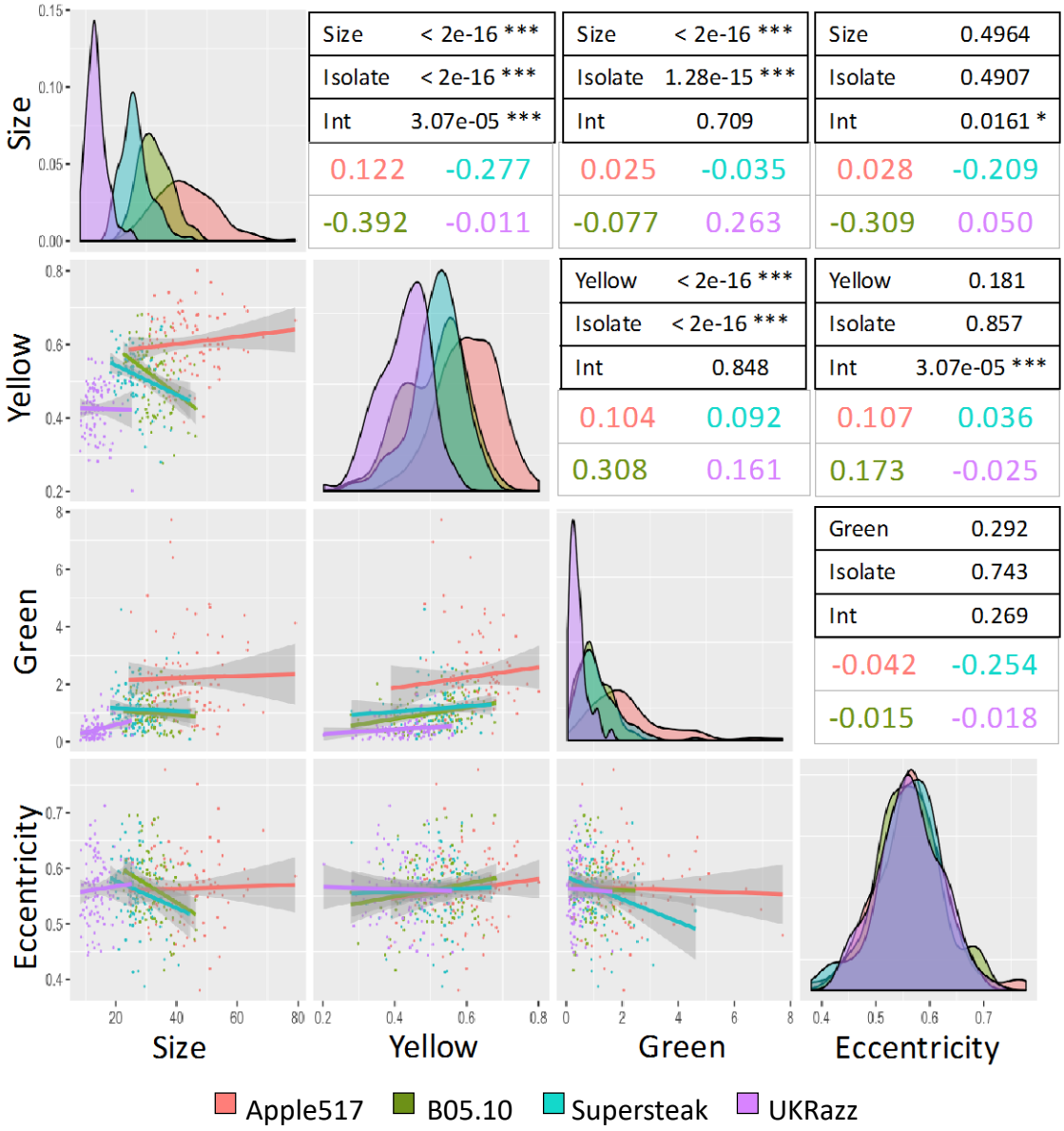

FIGURE 3 – Isolate dependency of Ttait correlations across the isolates

ANCOVA was used to test for correlations between each pair of traits across the 96 *A. thaliana* isolates using each of the four different *B. cinerea* isolates. Scatter plots with 95% confidence interval for the trait correlation in each isolate are shown on the left half of the plot. The diagonal shows the distribution of the specific trait across the four *B. cinerea* isolates. The right hand tables show the p-values for the trait-trait correlations, *B. cinerea* isolate dependency of these correlations, and the interaction of *B. cinerea* isolate on the trait-trait correlation (Int) using the following model). The estimated slopes for each trait-trait interaction for each *B. cinerea* isolate are shown by the colored text.

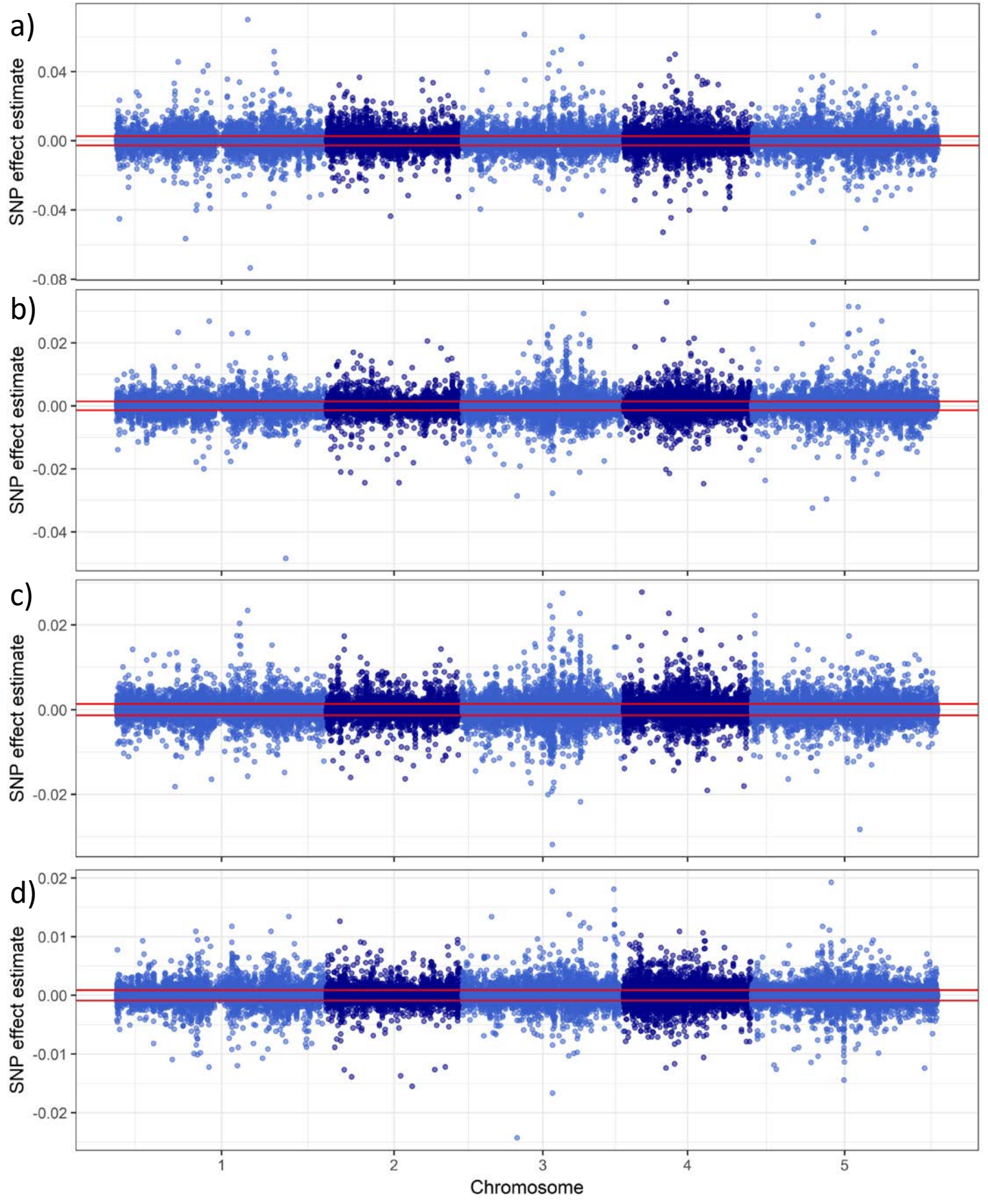

FIGURE 4 – Lesion size GWAS for four *B. cinerea* isolates

Manhattan plots showing the lesion size trait GWAS results, as measured on four *B. cinerea* isolates: a, Apple517; b, B05.10; c, Supersteak; and d, UKRazz. The horizontal red-line shows the significance threshold as estimated by permutation.

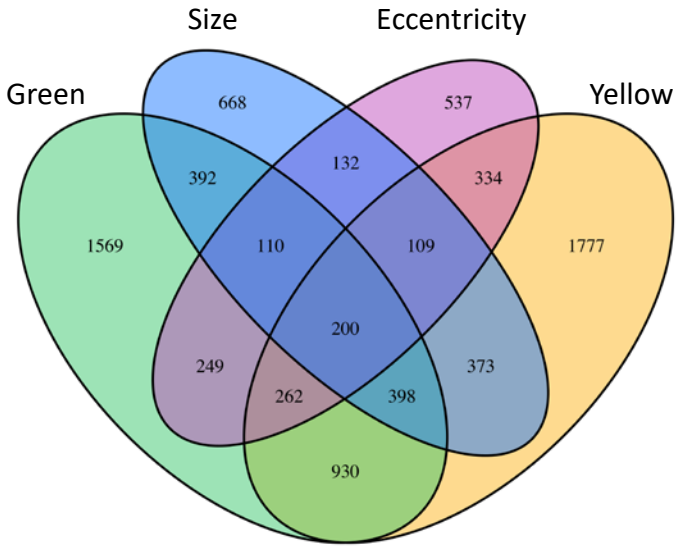

FIGURE 5 – Venn diagram of genes found in GWA mapping

A Venn diagram of the candidate *A. thaliana* genes found to associate with each lesion trait via GWA. The number of genes listed for each lesion trait reflects the number of genes with two or more SNPs above the 95th percentile threshold for that particular trait.

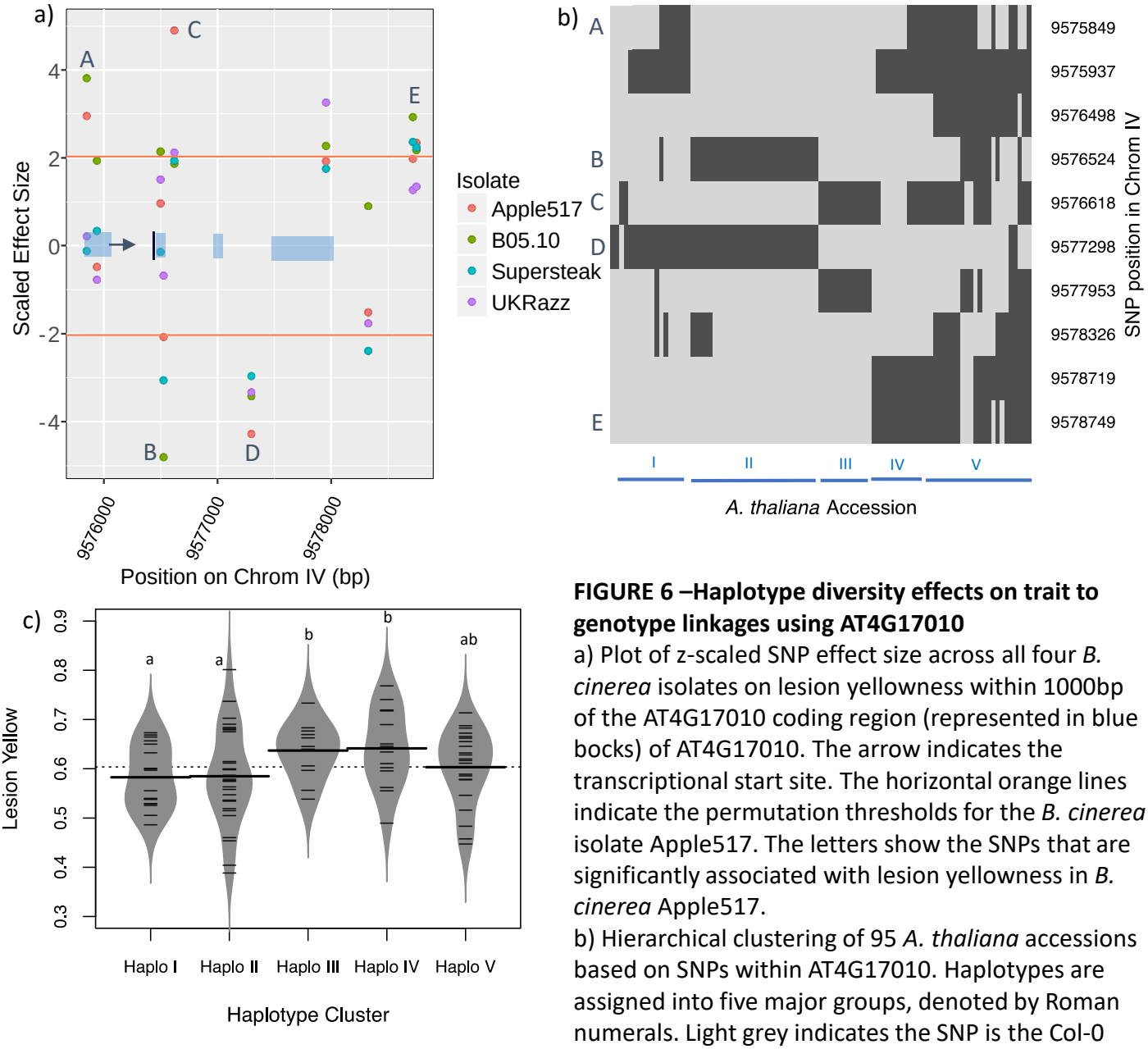

FIGURE 6 –Haplotype diversity effects on trait to genotype linkages using AT4G17010

a) Plot of z-scaled SNP effect size across all four *B. cinerea* isolates on lesion yellowness within 1000bp of the AT4G17010 coding region (represented in blue bocks) of AT4G17010. The arrow indicates the transcriptional start site. The horizontal orange lines indicate the permutation thresholds for the *B. cinerea* isolate Apple517. The letters show the SNPs that are significantly associated with lesion yellowness in *B. cinerea* Apple517.

b) Hierarchical clustering of 95 *A. thaliana* accessions based on SNPs within AT4G17010. Haplotypes are assigned into five major groups, denoted by Roman numerals. Light grey indicates the SNP is the Col-0 allele while dark grey is the opposite allele. The SNPs are presented in their genomic order rather than the haplotype grouped structure.

c) Distributions of lesion yellowness across the *A. thaliana* accessions infected with *B. cinerea* Apple517. The *A. thaliana* accessions are grouped by approximate SNP haplotypes in b. The model corrected mean value of lesion yellowness for *A. thaliana* reference accession Col-0 was 0.545. Significance differences between the groups are shown by letters.

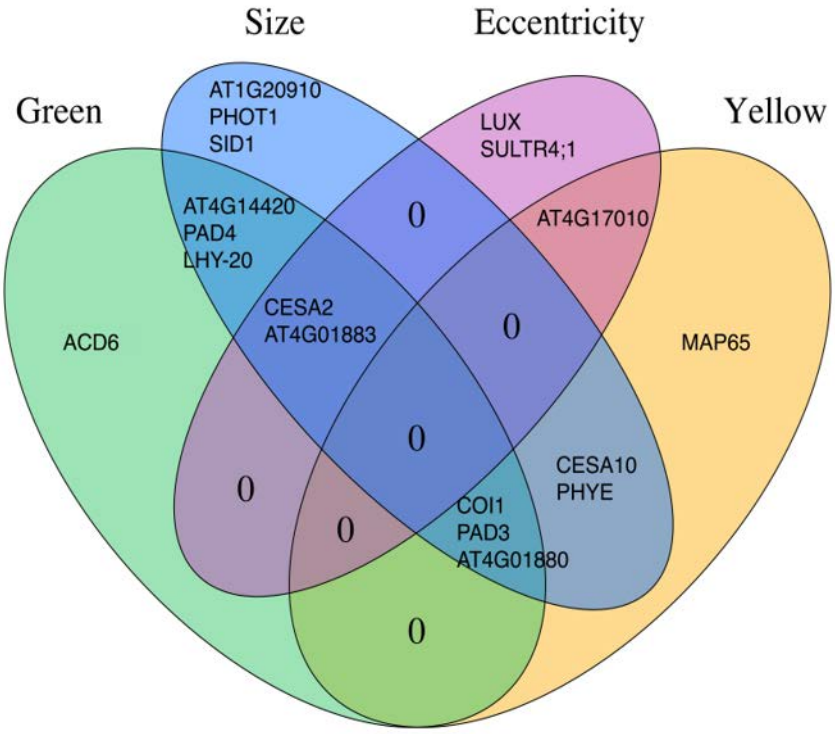

FIGURE 7 – Lesion traits affected by T-DNA insertional mutants

A Venn diagram showing the lesion traits significantly affected by each of the T-DNA knockout mutants in comparison to the wildtype background. The gene identifiers are located within the appropriate section of the diagram showing all the phenotypes altered by mutations in that gene.

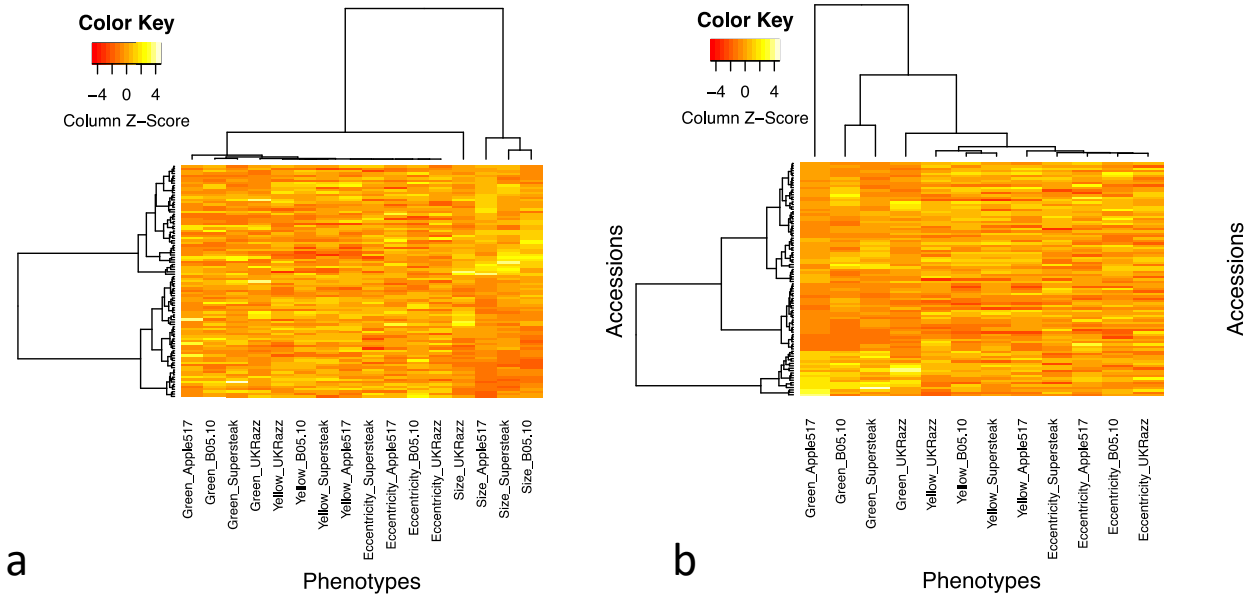

Figure S1: Hierarchical Cluster Analysis of Lesion Traits
Hierarchical cluster analysis of the a) four traits chosen to represent broad visual aspects of lesions, across the four pathogen isolates. b) Detail showing only color and shape traits illustrates relatedness and variation across accessions and isolates.

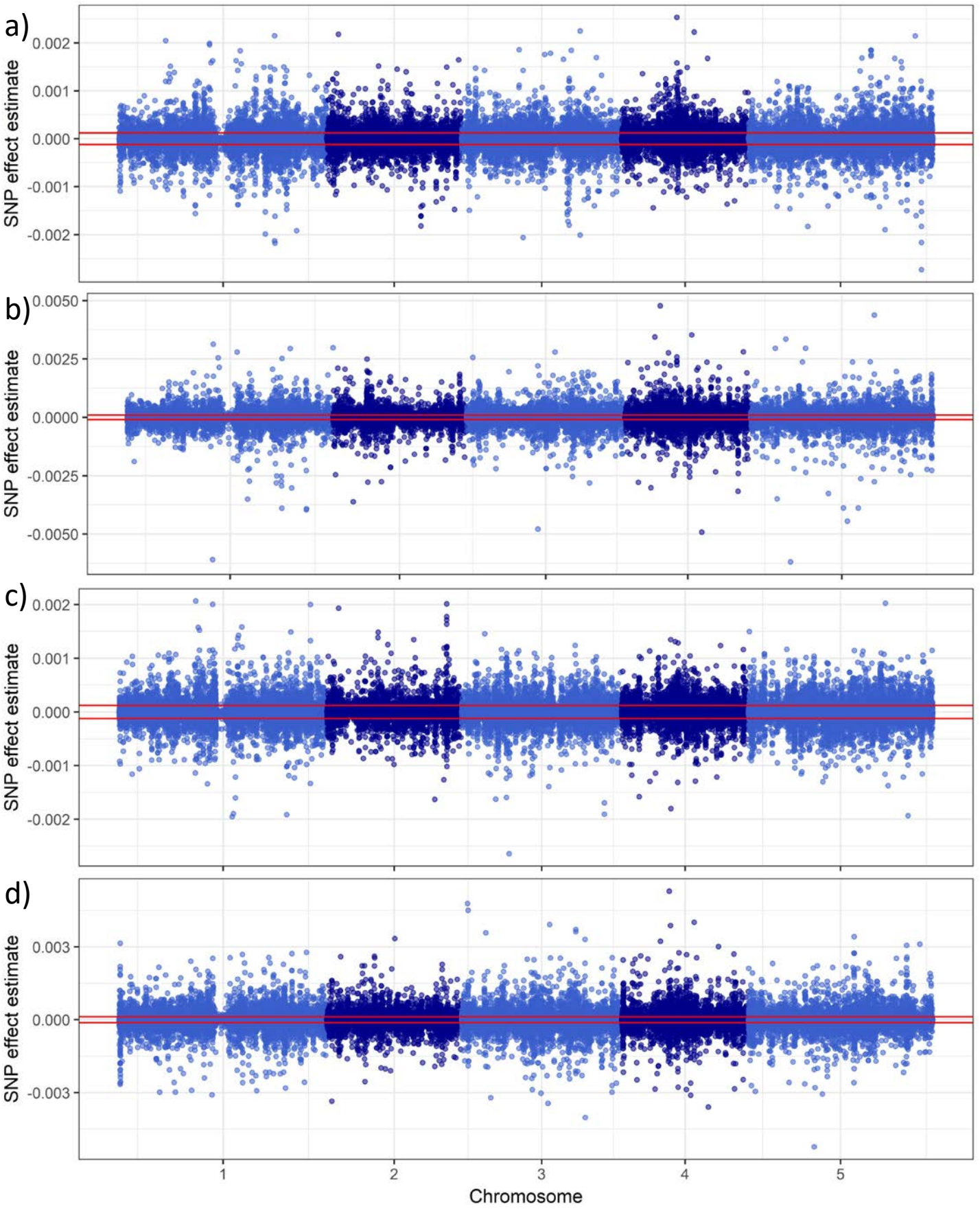

Figure S2: Lesion Greenness Manhattan Plots

Manhattan plots showing lesion greenness trait GWAS results, as measured on four *B. cinerea* isolates: a, Apple517; b, B05.10; c, Supersteak; and d, UKRazz. The horizontal red-line shows the significance threshold as estimated by permutation.

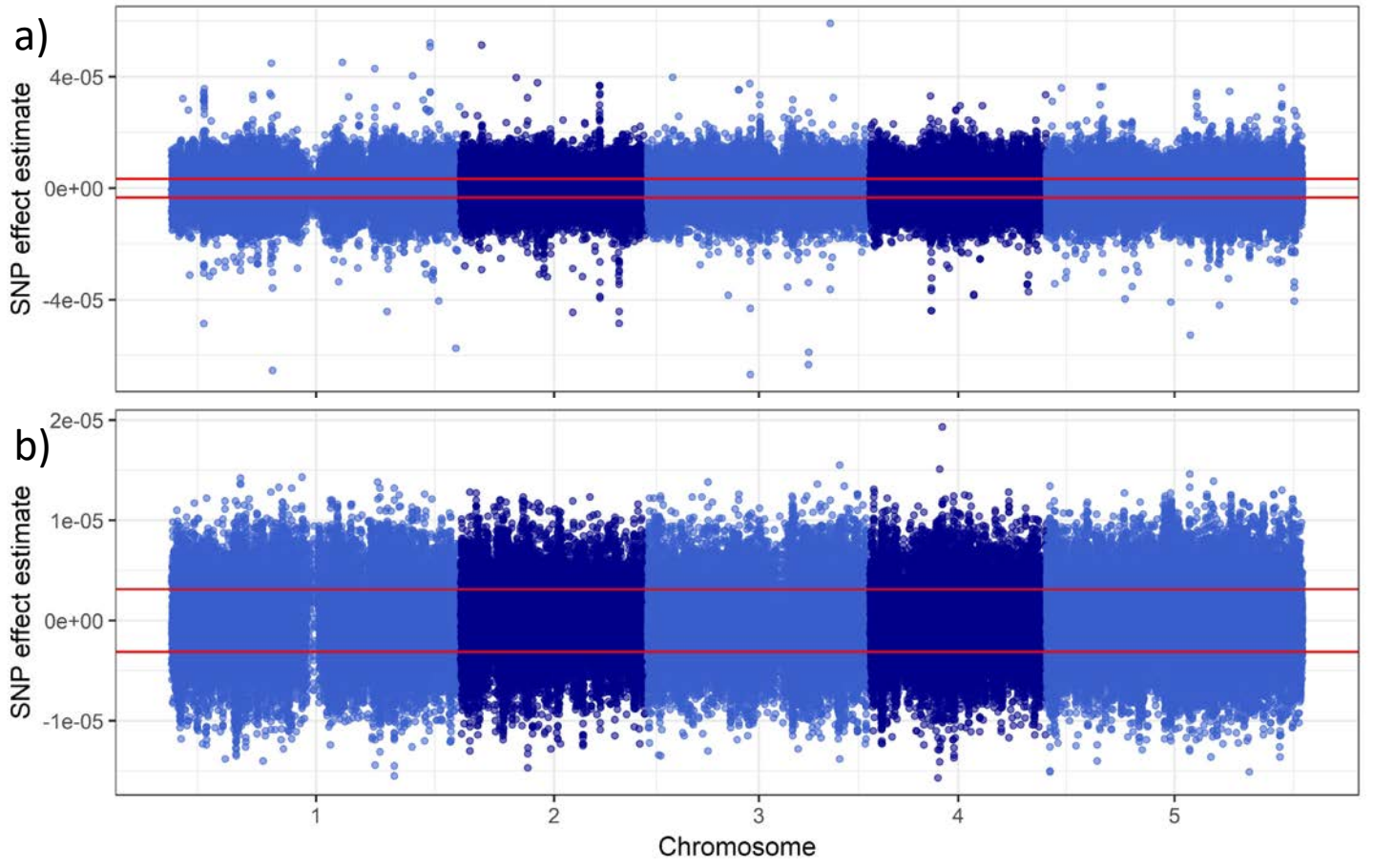

Figure S3: Lesion Yellowness and Eccentricity Shape Manhattan Plots for Apple517
Manhattan plots showing lesion yellowness (a) and eccentricity trait (b) GWAS results for Apple517. There were no significant SNPs identified for the other isolates. The horizontal red-line shows the significance threshold as estimated by permutation.